

High-phytate/low-calcium diet is a risk factor for crystal nephropathies, renal phosphate wasting, and bone loss

Ok-Hee Kim¹, Carmen J Booth², Han Seok Choi³, Jinwook Lee¹, Jinku Kang¹, June Hur¹, Woo Jin Jung¹, Yun-Shin Jung¹, Hyung Jin Choi⁴, Hyeonjin Kim⁵, Joong-Hyuck Auh⁶, Jung-Wan Kim⁷, Ji-Young Cha⁸, Young Jae Lee⁸, Cheol Soon Lee⁹, Cheolsoo Choi¹⁰, Yun Jae Jung¹¹, Jun-Young Yang¹², Seung-Soon Im¹³, Dae Ho Lee¹⁰, Sun Wook Cho¹⁴, Young-Bum Kim¹⁵, Kyong Soo Park¹⁴, Young Joo Park¹⁴, Byung-Chul Oh^{1*}

¹Department of Physiology, Lee Gil Ya Cancer and Diabetes Institute, Gachon University College of Medicine, Incheon, Republic of Korea; ²Department of Comparative Medicine, Yale University School of Medicine, New Haven, United States; ³Division of Endocrinology and Metabolism, Department of Internal Medicine, Dongguk University Ilsan Hospital, Goyang, Republic of Korea; ⁴Department of Anatomy, Seoul National University College of Medicine, Seoul, Republic of Korea; ⁵Department of Radiology, Seoul National University College of Medicine, Seoul, Republic of Korea; ⁶Department of Food Science and Technology, Chung-Ang University, Ansung, Republic of Korea; ⁷Department of Biology, University of Incheon, Incheon, Republic of Korea; ⁸Department of Biochemistry, Lee Gil Ya Cancer and Diabetes Institute Gachon University College of Medicine, Incheon, Republic of Korea; ⁹Medical Health Research Center, Korea University Anam Hospital, Seoul, Republic of Korea; ¹⁰Department of Internal Medicine, Gachon University Gil Medical Center, Incheon, Republic of Korea; ¹¹Department of Microbiology, Lee Gil Ya Cancer and Diabetes Institute, Gachon University College of Medicine, Incheon, Republic of Korea; ¹²Department of Toxicological Evaluation and Research, Ministry of Food and Drug Safety, Cheongju-si, Republic of Korea; ¹³Department of Physiology, Keimyung University School of Medicine, Daegu, Republic of Korea; ¹⁴Department of Internal Medicine, Seoul National University College of Medicine, Seoul, Republic of Korea; ¹⁵Division of Endocrinology, Diabetes, and Metabolism, Beth Israel Deaconess Medical Center and Harvard Medical School, Boston, United States

*For correspondence:
bcch@gachon.ac.kr

Competing interests: The authors declare that no competing interests exist.

Funding: See page 23

Received: 13 October 2019

Accepted: 22 March 2020

Published: 09 April 2020

Reviewing editor: Dolores Shoback, University of California, San Francisco, United States

© Copyright Kim et al. This article is distributed under the terms of the [Creative Commons Attribution License](https://creativecommons.org/licenses/by/4.0/), which permits unrestricted use and redistribution provided that the original author and source are credited.

Abstract Phosphate overload contributes to mineral bone disorders that are associated with crystal nephropathies. Phytate, the major form of phosphorus in plant seeds, is known as an indigestible and of negligible nutritional value in humans. However, the mechanism and adverse effects of high-phytate intake on Ca^{2+} and phosphate absorption and homeostasis are unknown. Here, we show that excessive intake of phytate along with a low- Ca^{2+} diet fed to rats contributed to the development of crystal nephropathies, renal phosphate wasting, and bone loss through tubular dysfunction secondary to dysregulation of intestinal calcium and phosphate absorption. Moreover, Ca^{2+} supplementation alleviated the detrimental effects of excess dietary phytate on bone and kidney through excretion of undigested Ca^{2+} -phytate, which prevented a vicious cycle of intestinal phosphate overload and renal phosphate wasting while improving intestinal Ca^{2+} bioavailability. Thus, we demonstrate that phytate is digestible without a high- Ca^{2+} diet and is a

risk factor for phosphate overloading and for the development of crystal nephropathies and bone disease.

Introduction

Phytate (*Myo*-inositol hexaphosphate) is the main phosphorus storage system in plant seeds such as those of cereal grains, nuts, oilseeds, and legumes (Raboy, 2000; Reddy et al., 1982), accounting for up to 80% of total phosphorus. Phytate tightly binds to essential minerals such as Ca^{2+} , Mg^{2+} , Fe^{2+} , and Zn^{2+} to form mineral-phytate salts because of its six phosphate groups (Kim et al., 2010; Oh et al., 2006). These mineral-phytate salts are known to be indigestible by monogastric animals and humans, which lack the digestive enzyme phytase that releases phosphate from mineral-phytate salts (Reddy and Sathé, 2002). The prevailing hypothesis argues that phytate-derived phosphorus is indigestible, not absorbed in the intestine, and is excreted in the feces (Golovan et al., 2001). This widespread belief led to the development of low-phytate crops and commercial phytases to improve the bioavailability of phytate-bound essential minerals, including phosphorus, and to improve the nutritional quality of plant seeds (Raboy, 2007). Thus, plant seeds or high-fiber vegetable proteins represent a poor or negligible source of bioavailable phosphate for intestinal absorption compared with animal proteins (Moe et al., 2011; Vervloet et al., 2017). Further, they are not considered to affect intestinal phosphate absorption adversely in humans eating diets that are mainly comprised of plant-based, cereal-rich diets (Reddy and Sathé, 2002). Nonetheless, there are insufficient data indicating the amount of phytate phosphorus that is bioavailable for intestinal absorption and whether specific conditions can modulate the bioavailability and digestibility of phytate.

High-phytate diets cause stronger adverse effects on Ca^{2+} , Fe^{2+} , and Zn^{2+} levels in infants, young children, and pregnant and lactating women when cereal-based foods represent a large percentage of the diet (Al Hasan et al., 2016; Chan et al., 2007). Prior studies of dogs demonstrate that increasing the levels of phytate reduces the intestinal absorption of Ca^{2+} and causes nutritional rickets (Harrison and Mellanby, 1939; Mellanby, 1949). Likewise, increasing dietary phytate is associated with secondary hyperparathyroidism in young adults because of the reduced intestinal absorption of dietary Ca^{2+} (Calvo et al., 1988; Pettifor, 1994). Consistent with previous observations (Ford et al., 1972; Goswami et al., 2000), a subsequent case-control study found that nutritional rickets is more prevalent in children who consume diets comprising low dietary Ca^{2+} and high phytate (Aggarwal et al., 2012). These findings suggest a strong association between high-phytate intake and metabolic bone diseases, including nutritional rickets and osteomalacia. However, although the roles of phytate in mineral deficiency are well-defined (Raboy, 2000; Reddy et al., 1982), who do not know whether dietary phytate can modulate the intestinal absorption of phosphate because of a lack of awareness.

Despite its adverse effects on animal and human health, dietary phytate can be beneficial because it inhibits digestive enzymes that hydrolyze lipids, proteins, and starch (Kumar et al., 2010). For example, high-phytate diets inhibit the absorption of glucose and lipids, leading to lower serum levels of glucose, triglycerides, and total cholesterol in humans (Thompson et al., 1987) and rodents (Kim et al., 2010; Jariwalla et al., 1990; Onomi et al., 2004). Moreover, diets based on vegetable protein lead to lower plasma levels of phosphate and fibroblast growth factor 23 (FGF23), a major regulator of phosphate homeostasis (Razzaque, 2009), compared with those based on meat protein (Moe et al., 2011). Indeed, few studies suggest that phytate diets reduce the risk of developing Ca^{2+} -induced kidney stones (Goswami et al., 2000). Unfortunately, these studies fail to contribute a broader understanding of the detrimental effects of excess phytate intake on the functions of bone and kidney, two major organs that regulate Ca^{2+} and phosphate homeostasis.

Here, we investigated the effects of excessive intake of phytate on Ca^{2+} and phosphate homeostasis in a rat model, as well as in a dietary study of humans. Thus, the goals of this study were to determine how a high-phytate diet affects kidney and bone health, to establish whether these changes depend on Ca^{2+} or mineral content, and to provide a rationale for restricting excessive phytate intake in patients who have kidney and metabolic bone diseases.

Results

Phytate-fed rats develop secondary hyperparathyroidism with hypophosphatemia and azotemia

We previously reported that phytate forms insoluble tricalcium- or tetracalcium-phytate salts in vitro over a wide pH range (Kim *et al.*, 2010). To evaluate the systemic effects of dietary phytate, rats (4-week-old male and female Sprague Dawley) were fed AIN-93G diets supplemented with 0% (control), 1%, 3%, or 5% phytate for 12 weeks (Figure 1A–Supplementary file 1). On the basis of the molecular weights of Ca^{2+} and phytate in these diets, increased phytate supplementation at a constant Ca^{2+} concentration (0.5%) gradually decreases the molar ratio of Ca^{2+} /phytate (Figure 1B). Rats that were fed higher levels of phytate (3% and 5%) exhibited decreased growth rates and reduced fat-free lean mass and whole-body fat compared with those of the control, despite similar daily food intake (Figure 1C–F). We reasoned therefore that the decreased growth rates were caused by decreased bioavailability of dietary Ca^{2+} associated with increased phytate supplementation.

To address this possibility, we used inductively coupled plasma mass spectroscopy (ICP-MS) to analyze fecal minerals. We found that dietary phytate led to the inhibition of intestinal absorption of essential minerals such as Ca^{2+} , Mg^{2+} , and Fe^{2+} in a concentration-dependent manner (Figure 1G–H, Figure 1—figure supplement 1A). Serum levels of Ca^{2+} remained within the normal range except in rats fed 5% phytate, which were associated with slightly reduced serum Ca^{2+} (Figure 1I). High-phytate-fed rats developed hypophosphatemia (Figure 1J) and hypomagnesemia (Figure 1K). Parathyroid hormone (PTH) levels markedly increased (5.4–11.7-fold) in the high-phytate groups by week 5 (Figure 1, Figure 1—figure supplement 1B) and remained elevated (2.8–6.4-fold) to week 12 (Figure 1L) in all phytate-fed rats because of sustained inhibition of intestinal Ca^{2+} absorption. These results suggest that PTH plays a role in the development of hypophosphatemia in high-phytate-fed rats.

Serum levels of creatinine (Cr) remained within the normal range except in rats fed 5% phytate, in which Cr levels were increased compared with controls (Figure 1, Figure 1—figure supplement 1C). By contrast, serum levels of blood urea nitrogen (BUN) showed a marked increase in rats fed high levels of phytate (3% and 5%) compared with controls (Figure 1M). The BUN/Cr ratio is a common laboratory value used to diagnose azotemia and acute kidney injury (Uchino *et al.*, 2012). Therefore, we determined the BUN/Cr ratio in phytate-fed rats. Rats exhibited a large increase in the BUN/Cr ratio in all phytate groups (Figure 1M, Figure 1—figure supplement 1D). Elevated BUN/Cr ratio may provide a biochemical signature of increased muscle catabolism associated with decreased fat-free lean mass in rats fed a high-phytate diet (Haines *et al.*, 2019). These results indicate that a high-phytate diet may lead to the development of azotemia.

Phytate-fed rats develop crystal nephropathies

To identify the cause of azotemia, we analyzed T2-weighted magnetic resonance images (MRI) of phytate-fed rats. MRI analysis revealed that rats fed 5% phytate had multiple renal cysts at the corticomedullary junction (Figure 2A, Figure 2—figure supplement 1A). The kidneys of these rats exhibited pronounced renomegaly with pitted, irregular, and granular cortices and medullar morphology (Figure 2—figure supplement 1B–C). The histopathological changes in the kidneys were evaluated while experimenters were blinded to the experimental group and scored for overall severity of renal injury, presence and severity of renal injury, Ca^{2+} deposits, and fibrosis. The severity of renal injury was greatest in female rats fed 3% or 5% phytate and in male rats fed 5% phytate, whereas control rats lacked significant pathological changes.

The presence and severity of nephrocalcinosis matched the severity of renal injury scores (Figure 2B–C). Pathological changes in phytate-fed rats were consistent with mild to severe crystal nephropathies (Mulay and Anders, 2017; Shavit *et al.*, 2015), including interstitial fibrosis, interstitial inflammation, tubular degeneration (ectasia, nephrocalcinosis, and protein casts), and enlarged or shrunken glomeruli (Figure 2D–F, Figure 2—figure supplement 1C–F). Alizarin Red S and von Kossa staining confirmed nephrocalcinosis, showing that the kidneys from phytate-fed rats contained extensive medullary Ca^{2+} deposits (Figure 2G). Interstitial fibrosis in phytate-fed rats was further confirmed using Masson's trichrome staining and immunohistochemical analysis of α -smooth muscle

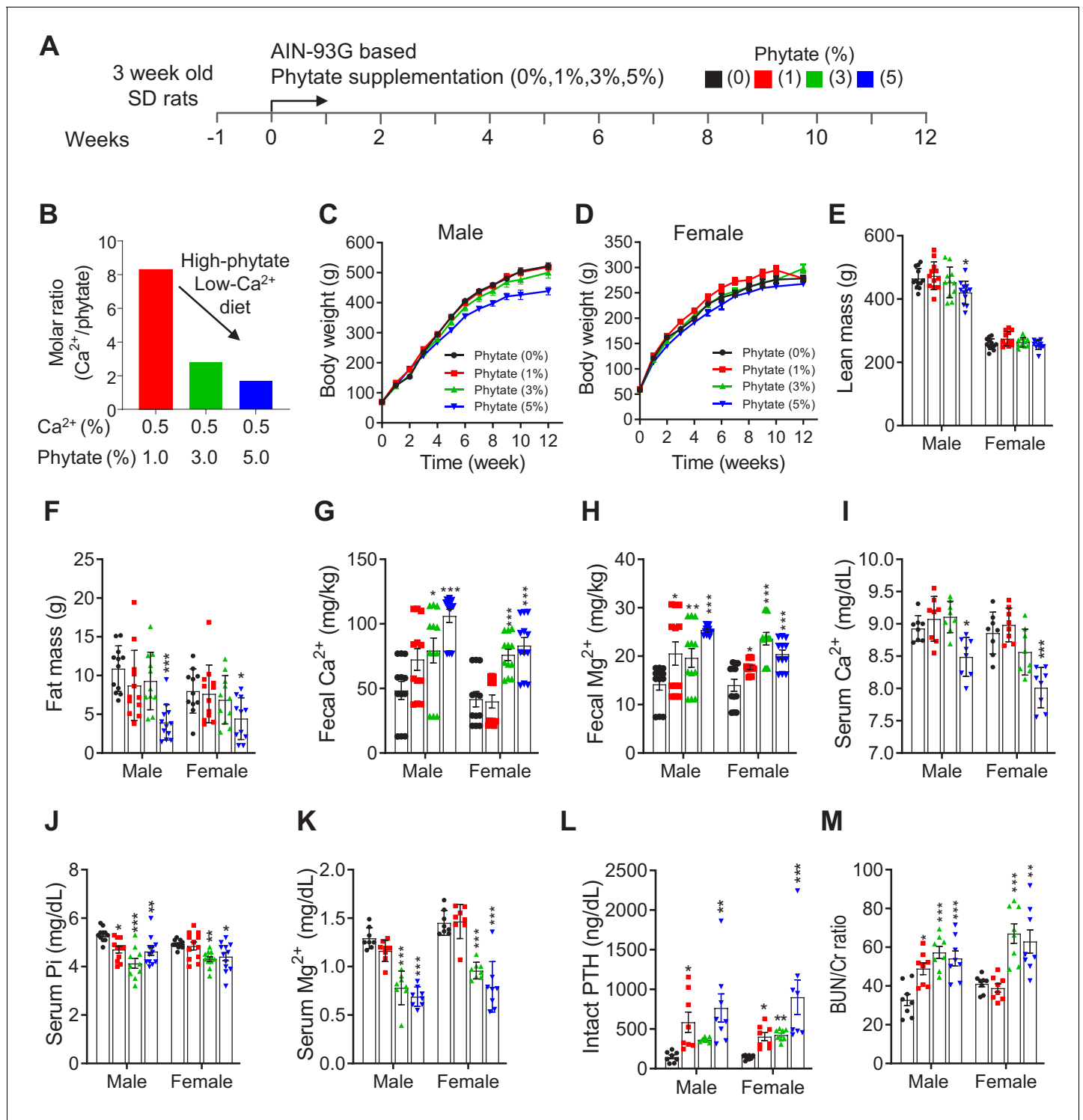


Figure 1. Phytate-fed rats develop secondary hyperparathyroidism with hypophosphatemia and azotemia. (A) Experimental design. After a 1-week period of adaptation with control AIN93G diet, we fed 4-week-old male and female Sprague–Dawley rats with AIN-93G diets supplemented with 0% (control), 1%, 3%, or 5% phytate for 12 weeks. (B) Molar ratio of Ca^{2+} to phytate content in the AIN93G diet (0.5% Ca^{2+}) supplemented with 1%, 3%, and 5% phytate. (C–D) Mean body weights of male (C) and female (D) rats of all groups after 12 weeks of feeding with the experimental diets. (E–F) Mean whole-body lean mass (E) and fat mass (F) values for all groups. Whole-body lean mass and fat mass were measured by nuclear magnetic resonance spectroscopy. (G–H) ICP-MS analysis of fecal excretion of Ca^{2+} (G) and Mg^{2+} (H) in all groups after 3 weeks of feeding with the experimental diets. (I–M) Serum levels of Ca^{2+} (I), phosphate (J), Mg^{2+} (K), intact PTH (L), and blood urea nitrogen (BUN)/Cr ratio (M) of all groups after 12 weeks of feeding with the experimental diets. Serum intact PTH levels were measured by enzyme-linked immunosorbent assay (ELISA). All comparisons were

Figure 1 continued on next page

Figure 1 continued

performed by one-way ANOVA with Tukey's post hoc multiple comparison test or the Kruskal–Wallis test (G, H, L) for non-parametric statistical analysis of data that did not have a normal distribution. The groups in panels G and H and 5% phytate in female rats failed the normality test, but no outliers were identified. Panel L failed the normality test, one sample of 3% phytate in male rats was out of range according to ROUT (Q = 1%), but it did not alter the statistical outcome and no data were excluded from that group. All data are presented as the mean ± standard deviation (SD) for each group (n = 8–12 per group). *p < 0.05, **p < 0.01, ***p < 0.001 compared with controls.

The online version of this article includes the following figure supplement(s) for figure 1:

Figure supplement 1. Metabolic characteristics of Sprague-Dawley rats fed control and phytate-supplemented diets.

actin, a marker of fibrosis (Figure 2H–I). Together, the histopathologic data demonstrate that a high-phytate diet resulted in marked renal injury with overt nephrocalcinosis and crystal nephropathy.

Phytate-fed rats develop severe bone loss

Growth retardation and metabolic bone disease are common in children and adolescents who have renal disease (Wesseling-Perry et al., 2012). To determine whether the phytate-fed rats developed skeletal changes and bone pathology coincident with renal disease, we performed dual-energy X-ray absorptiometry (pDEXA) and histological analyses of excised femora. Phytate-fed rats exhibited marked decreases in the rates of bone accrual along with decreased bone mineral density (BMD) in a concentration-dependent manner when compared with controls (Figure 3A). μ -CT images revealed concomitant increases in the bone marrow cavity space in phytate-fed rats compared with controls (Figure 3B). Further, phytate-fed rats exhibited significantly decreased trabecular bone volume (BV/TV), trabecular bone surface (BS/TV), trabecular number (Tb.N), and significantly increased trabecular space (Tb.Sp) compared with controls (Figure 3C). Consistent with the trabecular bone phenotypes, phytate-fed rats had markedly reduced cortical bone area (Tt.Ar) and increased cortical area fractions (Ct.Ar/Tt.Ar) (Figure 3D).

Male and female rats exhibited the same skeletal alterations, so we characterized the bone histopathology of the latter. Bone sections stained with toluidine blue showed that high-phytate diets decreased cartilage growth-plate thickness and bone osteoids (Figure 3E), consistent with skeletal alterations. Serum levels of receptor activator of nuclear factor kappa-B ligand (RANKL), a key component of osteoclastogenesis (Kong et al., 1999), were markedly increased in high-phytate-fed rats compared with controls (Figure 3F). The levels of osteoprotegerin (OPG), a RANKL decoy receptor that inhibits osteoclast differentiation and activation (Lacey et al., 1998), were significantly reduced (Figure 3G), and the sRANKL/OPG ratio was significantly increased in phytate-fed rats (Figure 3H). These data suggest a systemic acceleration of osteoclastogenesis in response to dietary phytate. Analysis of bone sections stained for tartrate-resistant acid phosphatase (TRAP) revealed that consumption of the high-phytate diet resulted in increased TRAP⁺ multinucleated cells (Figure 3I). Further, bone marrow-derived stromal cell cultures exhibited a significant concentration-dependent increase in the number of giant TRAP⁺ multinucleated osteoclasts (Figure 3J). Together, the data led us to posit that a high-phytate diet contributed to severe bone loss.

High-phytate diets dysregulate mineral and phosphate metabolism in humans

To determine whether our findings using rats were applicable to humans, we conducted a non-comparative pilot study to evaluate the short-term effects of phytate on six healthy premenopausal women (aged 23–34 years, body mass index, 17.7–25.8 kg/m²) (Figure 4A). The 12 day trial consisted of three consecutive diet cycles (four days in each cycle) of (1) polished white rice (WR, 0.35% phytate); (2) brown rice (BR, 1.07% phytate); and (3) brown rice with rice bran (BR+RB, 2.18% phytate; Supplementary file 2). At the end of each diet cycle, 16 hr fasting blood and 24 hr urine samples were collected from each participant. Serum levels of Ca²⁺, magnesium, and phosphate remained within the normal range for all three diets, although high dietary phytate intake was associated with slightly decreased serum phosphate levels (Figure 4B–C). Results for other biochemical parameters are summarized in Supplementary file 3.

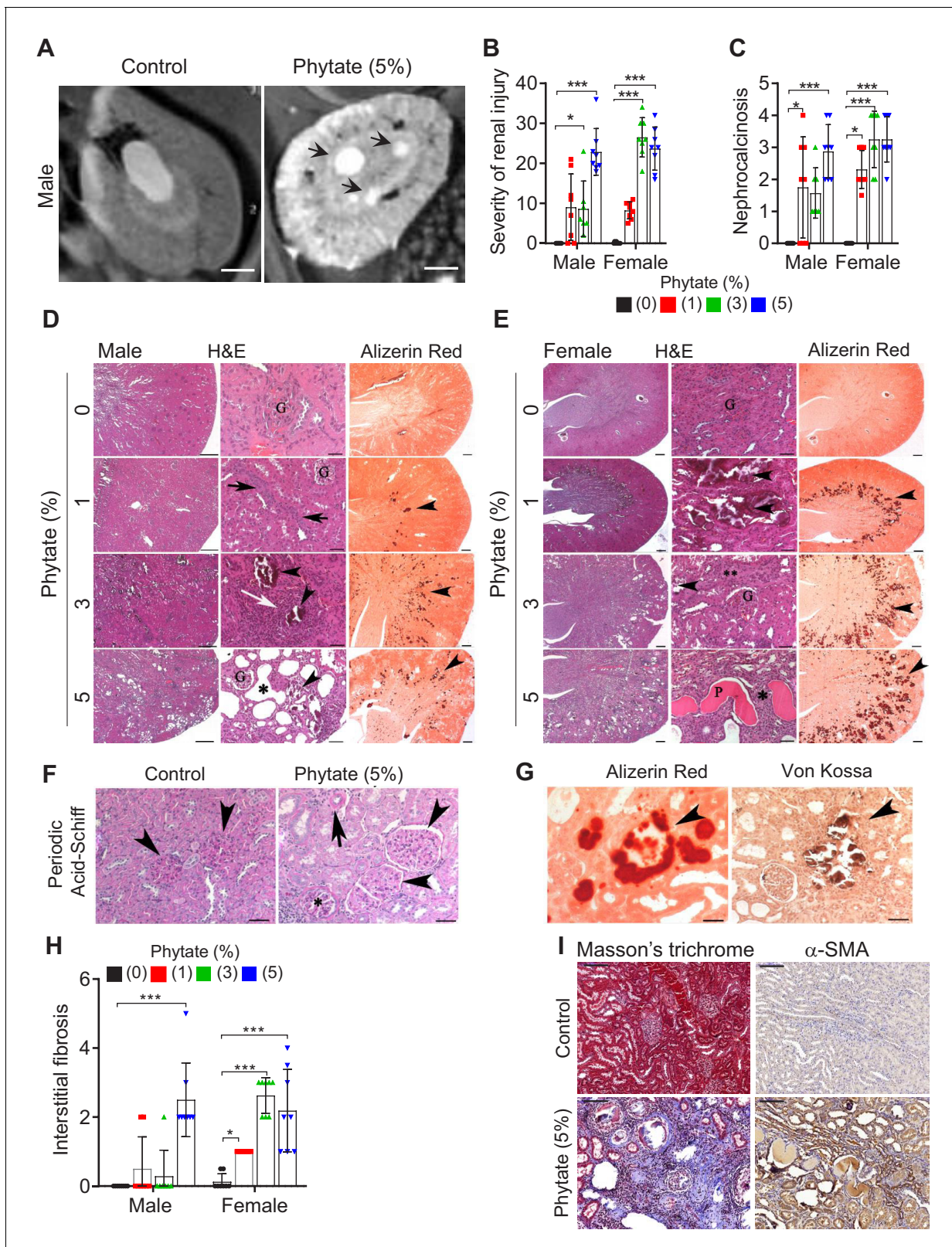


Figure 2. Phytate-fed rats develop crystal nephropathies. (A) Representative T2-weighted magnetic resonance images (MRIs) of kidneys from male rats fed a 5% phytate or control diet. The arrows point to kidney cysts in a phytate-fed rat. Scale bars, 250 μ m. (B–E) Kidney injury was examined by staining with hematoxylin and eosin, Alizerin Red S (AR), von Kossa (VK), or periodic acid-Schiff (PAS) staining. Scale bars in panels (D, E): left, 500 μ m; center, 50 μ m; right, 500 μ m. Granular material within the tubules (nephrocalcinosis) (arrowheads in panels [D, E]) was present in the kidneys of phytate-fed rats
Figure 2 continued on next page

Figure 2 continued

visualized using Alizarin Red S staining (D, E, right panels). Pathologic changes included tubular regeneration (black arrows), inflammation (white arrow), ectatic tubules (*), protein casts (P), interstitial fibrosis (**), and small shrunken glomeruli (G). (F) Representative PAS-stained sections from control (left) or phytate-fed (right) groups. (G) Calcification was detected using Alizarin Red S (left) and VK (right) stains. VK staining for Ca^{2+} was similar to that of Alizarin Red S (arrowheads). In phytate-fed rats with severe pathologic changes, glomeruli were often large (5% phytate, arrowheads) with increased PAS-positive material in the mesangium, Bowman's capsule of the glomeruli (*), and in the basement membrane of the tubules (arrow). Kidneys from control rats were unremarkable. Scale bar, 50 μm . (H, I) Interstitial fibrosis was further detected by staining with Masson's trichrome (H) or by immunohistochemistry using antibodies against α -smooth muscle actin (I). Scale bar, 100 μm . All comparisons were performed by one-way ANOVA, with Tukey's post hoc multiple comparison test or the Kruskal–Wallis test (B, C, H) for non-parametric statistical analysis of data that did not have a normal distribution. The groups in panels (G) and (H), as well as the 5% phytate in female rats, failed the normality test, but no outliers were identified. Panel (L) failed the normality test and one sample of 3% phytate in male rats was out of range according to ROUT ($Q = 1\%$), but it did not alter the statistical outcome and no data were excluded from that group. All data are presented as the mean \pm standard deviation (SD) for each group ($n = 8$ –12 per group). *, $p < 0.05$; **, $p < 0.01$; ***, $p < 0.001$ compared with controls.

The online version of this article includes the following figure supplement(s) for figure 2:

Figure supplement 1. Histopathological features of the kidneys of phytate-fed rats.

Urinary pH levels decreased in a dose-dependent manner as the intake of phytate increased (Figure 4D). Higher dietary phytate intake resulted in a marked decrease in the 24 hr urinary Ca^{2+} creatinine clearance rate (Figure 4E), whereas the 24 hr urinary phosphate creatinine clearance rate was only slightly increased (Figure 4F). These findings are consistent with the results of the tubular reabsorption rate, where high dietary phytate increases the renal tubular Ca^{2+} reabsorption rate (Figure 4G) but decreases the renal tubular phosphate reabsorption rate (Figure 4H). These metabolic characteristics are probably secondary to the increased levels of PTH that occur in response to high levels of dietary phytate intake (Figure 4I). Further, high dietary phytate decreased the serum levels of FGF23 (Figure 4—figure supplement 1A). Thus, we propose that the high dietary phytate intake dysregulates mineral and phosphate metabolism in humans in a manner consistent with the findings of our rat studies.

Ca^{2+} supplementation protects phytate-fed rats from renal phosphate wasting through the formation of indigestible Ca^{2+} -phytate salts

Our study showed that diets containing >2–3% phytate dysregulate Ca^{2+} and phosphate homeostasis in rats as well as in humans. Thus, when we calculated the daily amount of consumption of 3% phytate in rats, we found that administering 150–300 mg/kg phytate per day was harmful to rats. This daily dose range of phytate may correspond to 24.2–48.4 mg/kg body weight of humans (1,451–2,900 mg/60 kg) according to a simple practice guide for dose conversion between animals and humans (Nair and Jacob, 2016). This calculated daily dose range of dietary phytate represents an average intake that is greater than four-fold higher than those in the United States and the United Kingdom (631–746 mg) (Ellis et al., 1987).

Phytate binds Ca^{2+} with high affinity at physiological pH (Kim et al., 2010; Reddy and Sathe, 2002). Consequently, the detrimental effects of phytate only occur when a diet poor in trace elements or Ca^{2+} is consumed (Raboy, 2007; Humer et al., 2015). We asked therefore whether increasing the molar ratio of Ca^{2+} /phytate can modulate the bioavailability and digestibility of phytate in vivo. To address this question, we fed female rats a diet of 3% phytate supplemented with high (1%) Ca^{2+} (high phytate with high Ca^{2+} [HP-H Ca^{2+}]) to increase the molar ratio of Ca^{2+} /phytate and Ca^{2+} bioavailability compared with that provided by 3% phytate supplemented with low (0.5%) Ca^{2+} (high phytate with low Ca^{2+} [HP-L Ca^{2+}]) (Figure 5A—Supplementary file 1). The growth rates of rats fed the HP-H Ca^{2+} diet were decreased and not associated with significant changes in serum levels of Ca^{2+} , despite slightly higher food and water intake compared with controls (Figure 5—figure supplement 1A–D). Moreover, rats fed the HP-H Ca^{2+} diet completely normalized their serum levels of phosphate and BUN, as well as the BUN/Cr ratio compared with rats fed the HP-L Ca^{2+} diet (Figure 5B–C, Figure 5—figure supplement 1E), indicating that supplementation with high Ca^{2+} ameliorated hypophosphatemia and azotemia.

To identify the mechanism of phytate-induced hypophosphatemia, we collected 24 hr urine samples from phytate-fed rats. Rats fed the HP-L Ca^{2+} diet had markedly decreased urine pH (Figure 5—figure supplement 1F) without significant differences in urine volume (Figure 5—figure

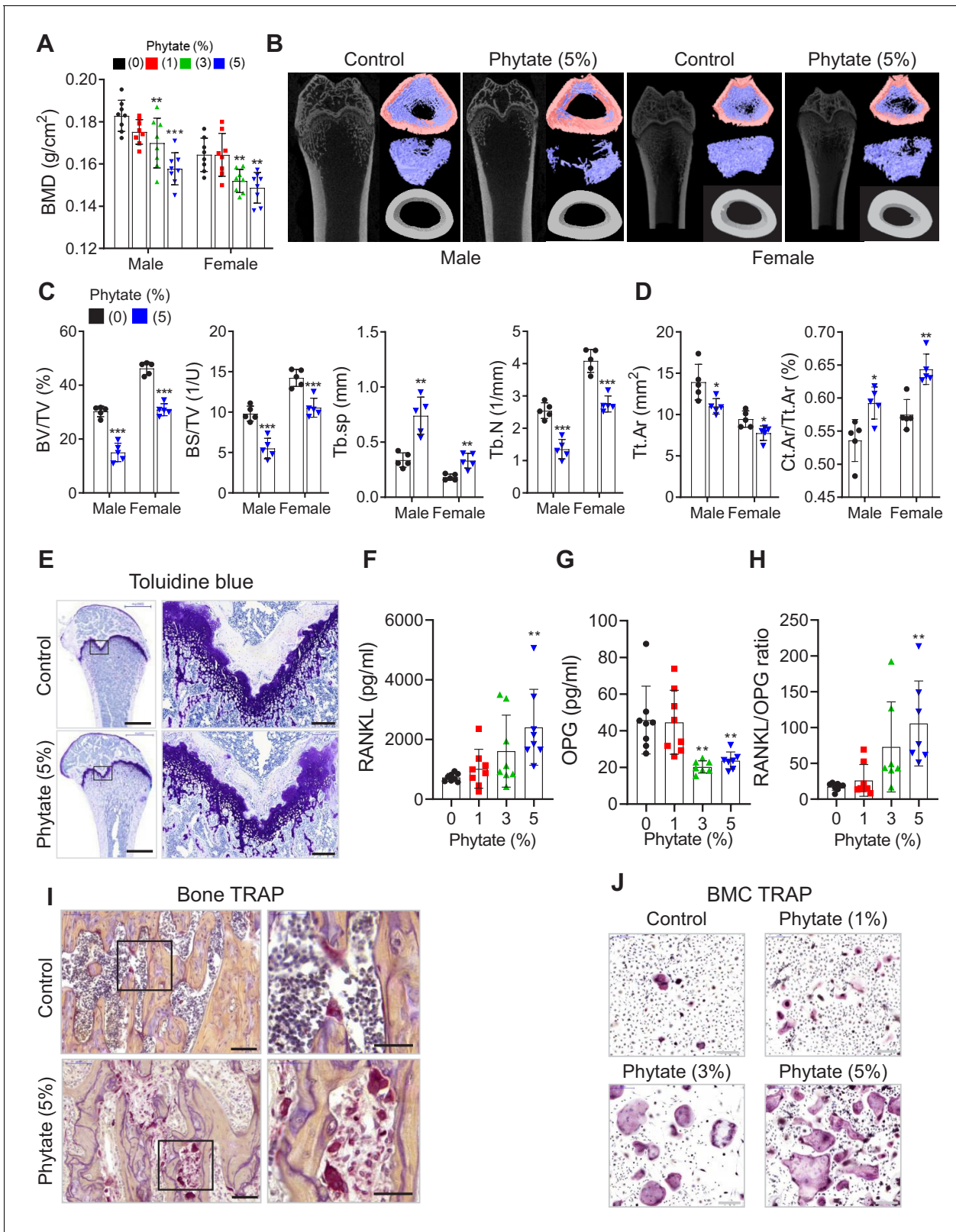


Figure 3. Phytate-fed rats develop severe bone loss. (A) Bone mineral density (BMD) was examined using peripheral dual-energy X-ray absorptiometry (pDEXA) of whole femora from rats fed control or phytate-supplemented diets (n = 8 per group). (B) Three-dimensional reconstructed μ -CT images of distal femora of rats fed control or phytate-supplemented diets. (C) Analysis of secondary spongiosa of the distal femur: bone volume fractions (BV/TV), bone surface density (BS/TV), trabecular separation (Tb.Sp), and trabecular number (Tb.N). (D) Analysis of the cortical bone of the distal femur: total Figure 3 continued on next page

Figure 3 continued

cross-sectional area inside the periosteal envelope (Tt.Ar) and cortical area fraction (Ct.Ar/Tt.Ar). (E) Representative toluidine blue-stained sections of decalcified femora from female rats fed control or phytate-supplemented diets. Scale bars: left, 1000 μm ; right, 100 μm . (F–H) Serum levels of soluble RANKL (F), OPG (G), and sRANKL/OPG ratio (H) in female rats fed control or phytate-supplemented diets. Serum sRANKL and OPG were measured using an ELISA ($n = 8$ per group). (I) Representative images of tartrate-resistant acid phosphatase (TRAP)-stained, EDTA-decalcified femur sections of rats fed control (upper) or phytate-supplemented (lower) diets. Red reaction product represents TRAP⁺ multinucleated osteoclasts. Scale bars: left, 500 μm ; right, 100 μm . (J) Bone marrow macrophages of rats fed control or phytate-supplemented diets for 12 weeks were cultured with RANK and macrophage colony-stimulating factor for 5 days. Osteoclasts were stained to detect TRAP activity. Scale bars: 200 μm . Comparisons were performed by unpaired Student's *t* test (C, D), one-way ANOVA with Tukey's post hoc multiple comparison test (F–H), or the Kruskal–Wallis test (C) for non-parametric statistical analysis of data that did not have a normal distribution. The HP-LCa²⁺ diet group in panel (C) failed the normality test, but no outliers were identified. All data are presented as the mean \pm SD of each group ([C, D] 0% and 5% phytate, $n = 5$ per group; [F–H] $n = 8$ per group). *, $p < 0.05$; **, $p < 0.01$; ***, $p < 0.001$ compared with controls.

supplement 1G), marked decreases in the 24 hr urinary Ca²⁺/Cr ratio (**Figure 5D**), and a marked increase in the 24 hr urinary Pi/Cr ratio (**Figure 5E**) compared with controls. Further, rats fed the HP-LCa²⁺ diet had markedly higher renal tubular reabsorption of Ca²⁺ (TmCa²⁺/GFR), with lower renal tubular reabsorption of phosphate (TmP/GFR) compared with controls (**Figure 5F–G**). Furthermore, rats fed the HP-LCa²⁺ diet had a markedly increased 24 hr urinary protein/Cr ratio compared to controls, suggesting that a high-phytate diet contributes to the development of proteinuria, a sign of renal damage (**Figure 5—figure supplement 1H**). We surmised that the high-phytate diet decreased urinary Ca²⁺ excretion while increasing renal phosphate wasting. Impaired renal Ca²⁺ and phosphate reabsorption are restored in rats fed the HP-HCa²⁺ diet (**Figure 5F–G**).

High-performance ion chromatographic (HPIC) analysis of feces demonstrated that rats fed the HP-HCa²⁺ diet excreted an approximately three-fold higher level of fecal phytate compared with rats fed the HP-LCa²⁺ diet (**Figure 5H–I**). ICP-MS analysis, performed after acid hydrolysis of fecal phytate to generate phosphate, further confirmed that rats fed the HP-HCa²⁺ diet exhibited an approximately 3.8-fold greater increase in Ca²⁺ and phosphate excretion compared with rats fed the HP-LCa²⁺ diet (**Figure 5J–K**), confirming findings of increased fecal excretion of undigested Ca²⁺-phytate in rats fed the HP-HCa²⁺ diet. Thus, we conclude that rats fed the HP-HCa²⁺ diet accumulated unabsorbed and indigestible Ca²⁺-phytate salts in the intestine while decreasing the intestinal phosphate available for absorption, indicating that the endogenous enzyme phytase was unable to hydrolyze Ca²⁺-phytate salts.

Conversely, rats fed the HP-LCa²⁺ diet hydrolyzed and absorbed >68–74% of the phosphate in the intestine (**Figure 5H–K**) with a concomitant increase in urinary phosphate excretion, thus developing renal phosphate wasting (**Figure 5E–G**). These data indicate that rats that were fed the HP-LCa²⁺ diet exhibited increased intestinal phosphate overloading caused by excessive phytate hydrolysis, which is consistent with evidence indicating that renal excretion of phosphate increases when phosphate intake is excessive (Vervloet et al., 2017). As phosphate and Ca²⁺ uptake occur along the gastrointestinal tract via the dedicated phosphate channel NaPi-2b and the major Ca²⁺ channel TRPV6, we analyzed the expression levels of NaPi-2b and TRPV6 in the intestinal tissues by immunohistochemical staining. However, there were no differences in expression levels of intestinal NaPi-2b or TRPV6 between any of the different dietary groups (**Figure 5—figure supplement 2A–D**). Thus, our findings demonstrate that phytate was digestible and absorbed in the intestine, considering that phytate is indigestible and unabsorbable in vivo when it forms Ca²⁺-phytate salts in the presence of high Ca²⁺ concentrations. Further, these findings are consistent with those of our previous in vitro studies (Kim et al., 2010).

Changes in the microbiota of phytate-fed rats and the expression levels of intestinal multiple inositol polyphosphate phosphatase as a potential phytase

Given that phytate is digestible in the presence of low-Ca²⁺ diets but is indigestible in the presence of high Ca²⁺ diets in vivo, we examined whether phytate can be hydrolyzed by phytases from either intestinal microbiota or intestinal tissues. To address this question, we analyzed the predominant bacteria in rat feces by quantitative real-time PCR for 16S rDNA using a set of phylum- and class-specific primers (**Supplementary file 4**) for *Firmicutes*, *Bacteroidetes*, β -*Proteobacteria*, and

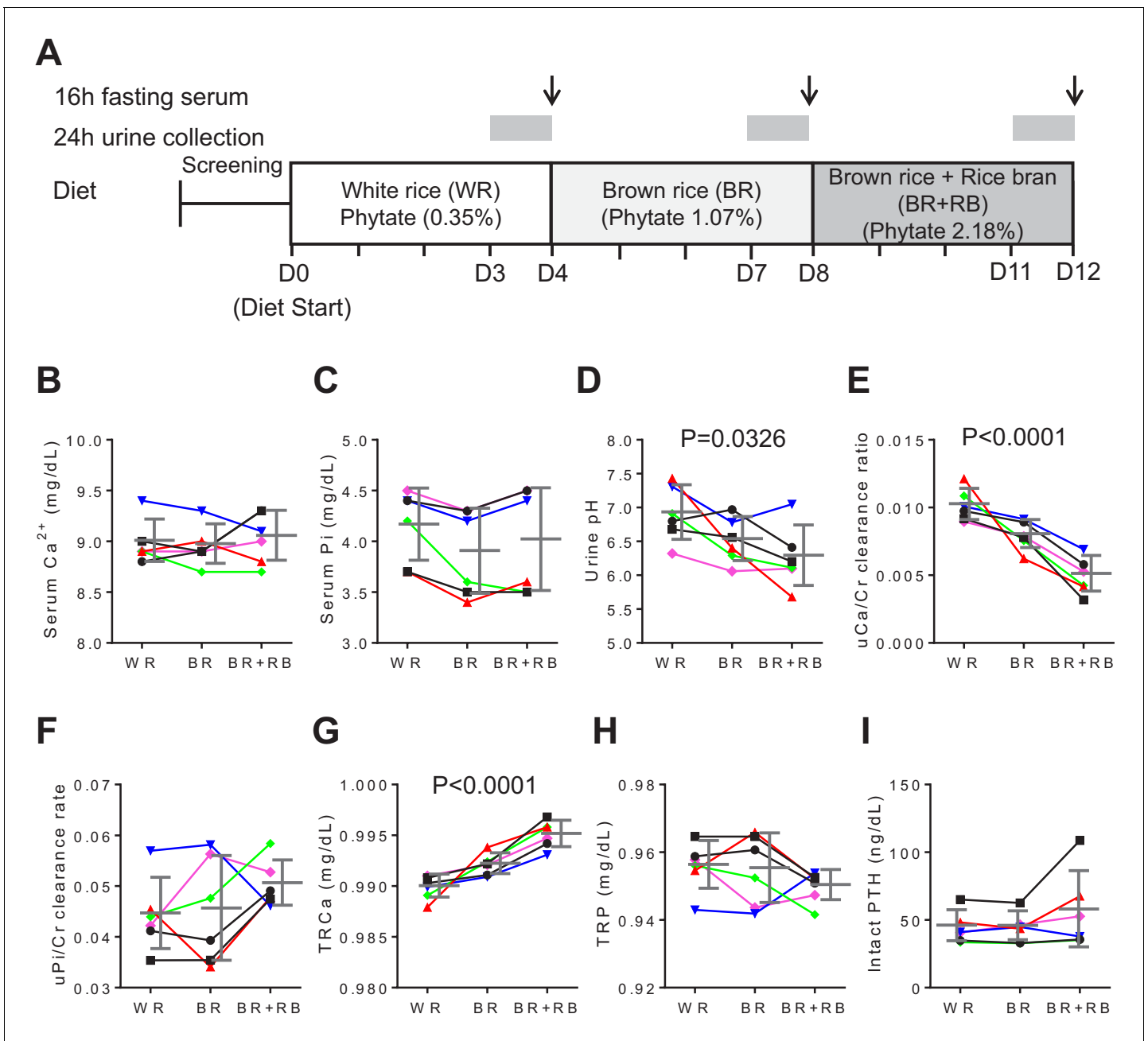


Figure 4. High-phytate diets dysregulate mineral and phosphate metabolism in humans. (A) Experimental design (six healthy female volunteers). (B, C) Time course of serum levels of Ca^{2+} (B) and phosphate (C) for three different phytate doses. (D–H) Kinetics of urine pH (D), 24 hr urine Ca^{2+}/Cr ratio (E), 24 hr urine Pi/Cr ratio (F), renal tubular Ca^{2+} reabsorption (TRCa) (G), and renal tubular phosphate reabsorption (TRP) (H) for three different phytate doses. (I) Time-course analysis of serum levels of intact PTH for different phytate doses. Data are presented as the mean \pm SD for each dose ($n = 6$ per dose). Statistical significance was tested by repeated measure ANOVA between subjects and groups. All data are presented as the mean \pm SD for each dose ($n = 6$ per dose).

The online version of this article includes the following figure supplement(s) for figure 4:

Figure supplement 1. High-phytate diets dysregulate mineral and phosphate metabolism in humans.

Actinobacteria. Phylum-level analysis indicated that rats fed the HP-LCa²⁺ diet had significantly higher levels of *Firmicutes*, *Bacteroidetes*, and β -*Proteobacteria*, but had markedly lower levels of *Actinobacteria* compared to controls (Figure 5—figure supplement 2E–H). Interestingly, the relative abundance of *Bacteroidetes* and β -*Proteobacteria* had markedly increased, whereas the relative

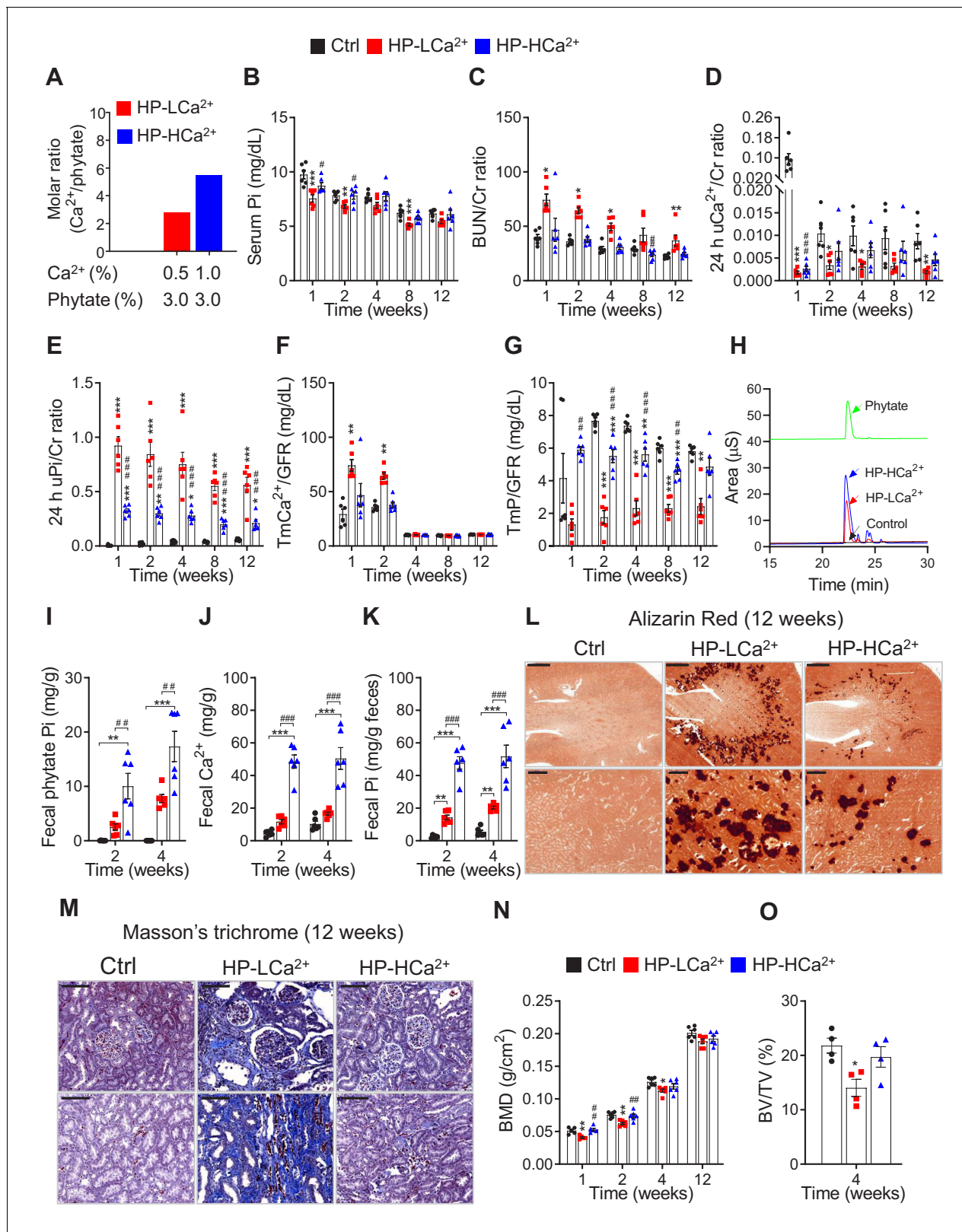


Figure 5. Ca^{2+} supplementation protects phytate-fed rats from renal phosphate wasting disorders, crystal nephropathies, and bone loss via indigestible Ca^{2+} -phytate salts. (A) Molar ratio of Ca^{2+} to phytate content when the diet was supplemented with 1.0% Ca^{2+} . (B–C) Time-course analysis of serum Pi level (B) and BUN/Cr ratio (C) in rats fed control, HP-LCa²⁺, and HP-HCa²⁺ diets for 12 weeks. (D–G) Time-course analysis of 24 hr urinary Ca^{2+} /Cr ratio (D), 24 hr urinary Pi/Cr ratio (E), ratio of tubular maximum reabsorption rate of renal tubular Ca^{2+} to glomerular filtration rate (TmCa²⁺/GFR) (F), and Figure 5 continued on next page

Figure 5 continued

ratio of tubular maximum reabsorption of renal tubular phosphate to glomerular filtration rate (TmP/GFR) (G) in all groups during 12 weeks of experimental feeding. (H) Representative data of fecal phytate analysis by HPLC. (J–K) Time-course analysis of fecal Ca²⁺ (J) and Pi (K) by ICP-MS in all groups after 2 and 4 weeks. Fecal phytate phosphorus was calculated as follows: [Phytate Pi] = [(Pi) from rats fed phytate diets] – [(Pi) from rats fed control diet]. (L–M) Representative data of Alizarin Red S staining (L) and Masson's trichrome staining (M) of kidney sections in all groups after 12 weeks. (N–O) Bone mineral density (BMD) (N) and bone surface/volume ratio (BS/BV) (O) in all groups. All comparisons were conducted by one-way ANOVA with Tukey's post hoc multiple comparison test. All data are presented as the mean ± SD for each group (n = 4–6 per group). *, p<0.05; **, p<0.01; ***, p<0.001, compared with controls. #, p<0.05; ##, p<0.01; ###, p<0.001, compared with HP-LCa²⁺ diet group.

The online version of this article includes the following figure supplement(s) for figure 5:

Figure supplement 1. Ca²⁺ supplementation protects rats fed phytate from crystal nephropathies.

Figure supplement 2. The expression levels of intestinal MINPP1, TRPV6, and NaPi-2b and real-time PCR analysis of stool microbiota in rats fed control, HP-LCa²⁺, and HP-HCa²⁺ diets for 12 weeks.

Figure supplement 3. Ca²⁺ supplementation protects rats fed phytate from crystal nephropathies.

Figure supplement 4. Ca²⁺ supplementation protects phytate-fed rats from renal fibrosis and skeletal abnormalities.

abundance of *Firmicutes* had decreased in response to high-phytate diets (Figure 5—figure supplement 2I), suggesting that diets containing high-phytate altered the composition of the gut microbiota.

As we observed phytate hydrolysis in rats fed the HP-LCa²⁺ diet, we further investigated whether phytate hydrolysis is associated with either microbial or mammalian phytase activity. Although humans and other monogastric animals, such as pigs, chickens, mice, and rats, are known to lack or have low phytase activities capable of hydrolyzing dietary phytate (Iqbal et al., 1994), recent studies and data in biological databases, such as UniProtKB and the Human Protein Atlas, have suggested that multiple inositol polyphosphate phosphatase 1 (MINPP1) is a strong candidate as a histidine acid phytase in humans and other monogastric animals as well as in gut microbiota (Cho et al., 2006; Stentz et al., 2014). MINPP1 could be a secreted enzyme with extremely high catalytic activity for phytate and is widely expressed in several tissues, including the stomach, duodenum, small intestine, colon, and pancreas, as well as at the highest levels in kidney, liver, and placenta. Phylogenetic analysis of bacterial MINPP1 (Stentz et al., 2014) suggested that Bacteroidetes express and secrete a homolog of a mammalian MINPP1 in the gut, whereas Firmicutes, a major phylum of the human intestinal microbiota, do not encode a protein homolog of MINPP1 (Supplementary file 5). These results suggested that increased phytate hydrolysis in rats fed the HP-LCa²⁺ diet is associated with the increase in relative abundance of *Bacteroidetes* and the decrease in relative abundance of *Firmicutes* (Figure 5—figure supplement 2I). Consistent with microbiota changes, immunohistochemical analysis of mammalian intestinal MINPP1 demonstrated that rats show high levels of MINPP1 expression in the villi of the intestine. Importantly, rats fed the HP-HCa²⁺ diet had markedly increased levels of intestinal MINPP1 (Figure 5—figure supplement 2J–K), probably to increase the enzymatic activity against chronic indigestible Ca²⁺-phytate in the presence of a high Ca²⁺ concentration for 12 weeks. Taken together, these findings suggest crucial roles of gut bacterial and intestinal MINPP1 in the hydrolysis of dietary phytate, although further research is needed to determine whether the hydrolysis of phytate by MINPP1 is direct and/or indirect.

Ca²⁺ supplementation protects phytate-fed rats against crystal nephropathies and bone loss

We next examined the morphological and histopathological changes in bones and kidneys when rats were fed the HP-LCa²⁺ diet. Ca²⁺ supplementation protected these rats against the development of the expected severe gross and microscopic changes of renomegaly (Figure 5—figure supplement 3A–B) and medullary nephrocalcinosis (Figure 5L, Figure 5—figure supplement 3D–F), respectively, as revealed by Alizarin Red S staining. However, we found no differences in serum levels of oxalate between diet groups (Figure 5—figure supplement 3G), suggesting that phytate-induced nephrocalcinosis was mainly with medullary calcium deposits, consistent with the findings of renal histology, such as Alizarin Red S and von Kossa staining. Further, rats that were fed the HP-HCa²⁺ diet expressed lower levels of four key markers (Kronenberg, 2009) of renal damage and fibrosis

(NGAL, COL1A1, COL6A2, and MPG) (Figure 5—figure supplement 4A) and exhibited decreased renal fibrosis revealed by Masson's trichrome staining to detect collagen (Figure 5M, Figure 5—figure supplement 4B–C). These data suggest that the HP-LCa²⁺ diet was a key contributor to renal damage and fibrosis. Further, pDEXA and μ -CT analyses of excised femora confirmed that rats fed the HP-HCa²⁺ diet were protected against the expected bone loss and demineralization observed in rats fed the HP-LCa²⁺ diet (Figure 5N–O, Figure 5—figure supplement 4D–G). Together, these findings support our hypothesis that high dietary phytate intake leads to damage of renal tissues as well as impaired bone mass accrual, whereas Ca²⁺ supplementation of the high-phytate diet has protective effects.

Phytate-mediated Ca²⁺ deficiency promotes vitamin D insufficiency and renal phosphate wasting independent of FGF23 expression

To identify the physiological mechanisms of high-phytate diets on vitamin D metabolism, we performed a time-course analysis of the serum levels of PTH, 25(OH)D, and activated vitamin D (1,25(OH)₂D). First, we found that the serum levels of PTH were consistently elevated in rats fed the HP-LCa²⁺ diet compared with control rats and rats fed the HP-HCa²⁺ diet (Figure 6A). Second, we found that rats fed the HP-LCa²⁺ diet in conjunction with high PTH had decreased serum levels of 25(OH)D compared with controls (Figure 6B), leading to increased serum levels of 1,25(OH)₂D (Figure 6C). In rats fed the HP-HCa²⁺ diet, the serum levels of 25(OH)D and 1,25(OH)₂D normalized, indicating that Ca²⁺ supplementation inhibited the metabolism of serum 25(OH)D to 1,25(OH)₂D (Figure 6B–C). Consistent with these findings, Ca²⁺ supplementation normalized the renal expression levels of CYP27B1, CYP24A1, and vitamin D receptor (VDR) (Figure 6D–F). Further, our findings, which are consistent with those of a previous study (Clements et al., 1987), demonstrate that phytate-mediated inhibition of intestinal Ca²⁺ absorption as well as increased phosphate overload promoted the metabolism of 25(OH)D to 1,25(OH)₂D, suggesting that high-phytate diets deplete serum 25(OH)D, which mitigates the harmful effects of phytate.

To identify proteins that contributed to phytate-mediated impairment of renal tubular Ca²⁺ and phosphate reabsorption, we analyzed the mRNA levels of key renal genes associated with Ca²⁺ and phosphate homeostasis, including those associated with Ca²⁺ channels, phosphate channels, and regulatory proteins (Mulay and Anders, 2017; Huang et al., 2013). We found that the renal expression of key genes associated with renal phosphate wasting, including those encoding Ca²⁺-sensing receptor (CaSR), inositol 1,4,5-trisphosphate receptor 1 (ITPR1), α Klotho, sodium/phosphate cotransporters (NaPi-2a and NaPi-2c), sodium-hydrogen antiporter 3 regulator 1 (NHERF1), and phosphate-regulating neutral endopeptidase X-linked, was markedly decreased in phytate-fed rats (Figure 6—figure supplement 1A). Each of these genes is associated with the development of nephrocalcinosis and renal phosphate wasting (Shavit et al., 2015; Huang et al., 2013; Karim et al., 2008; Monico and Milliner, 2012).

Immunoblot analysis further confirmed that the renal expression of α Klotho was significantly decreased in rats fed the HP-LCa²⁺ diet compared with controls (Figure 6G–H Figure 6—figure supplement 1B–C), suggesting that low levels of renal α Klotho may represent a complementary mechanism that increases serum phosphate levels in response to severe hypophosphatemia in rats fed the HP-LCa²⁺ diet. High serum FGF23 levels in conjunction with elevated levels of PTH contribute to the pathogenesis of renal phosphate wasting and hypophosphatemic rickets (Vervloet et al., 2017; Rodriguez-Ortiz et al., 2012; Walton and Bijvoet, 1975). Therefore, we analyzed the serum levels of FGF23. Unexpectedly, quantitative analysis did not detect significant changes in the serum levels of full-length FGF23 or its C-terminal FGF23 in rats fed the HP-LCa²⁺ diet compared with controls (Figure 6—figure supplement 1D–E). Immunoblot and immunohistochemical analyses of sections of the femur revealed that rats fed the HP-LCa²⁺ diet showed decreased levels of FGF23 in the calvarial bones (Figure 6I–J, Figure 6—figure supplement 1F), suggesting that the phytate-mediated renal phosphate wasting was mainly caused by high PTH levels independent of FGF23.

Discussion

Here, we show that the HP-LCa²⁺ diet was a significant risk factor for phosphate overloading and renal phosphate wasting associated with increased risks of nephrocalcinosis, renal fibrosis,

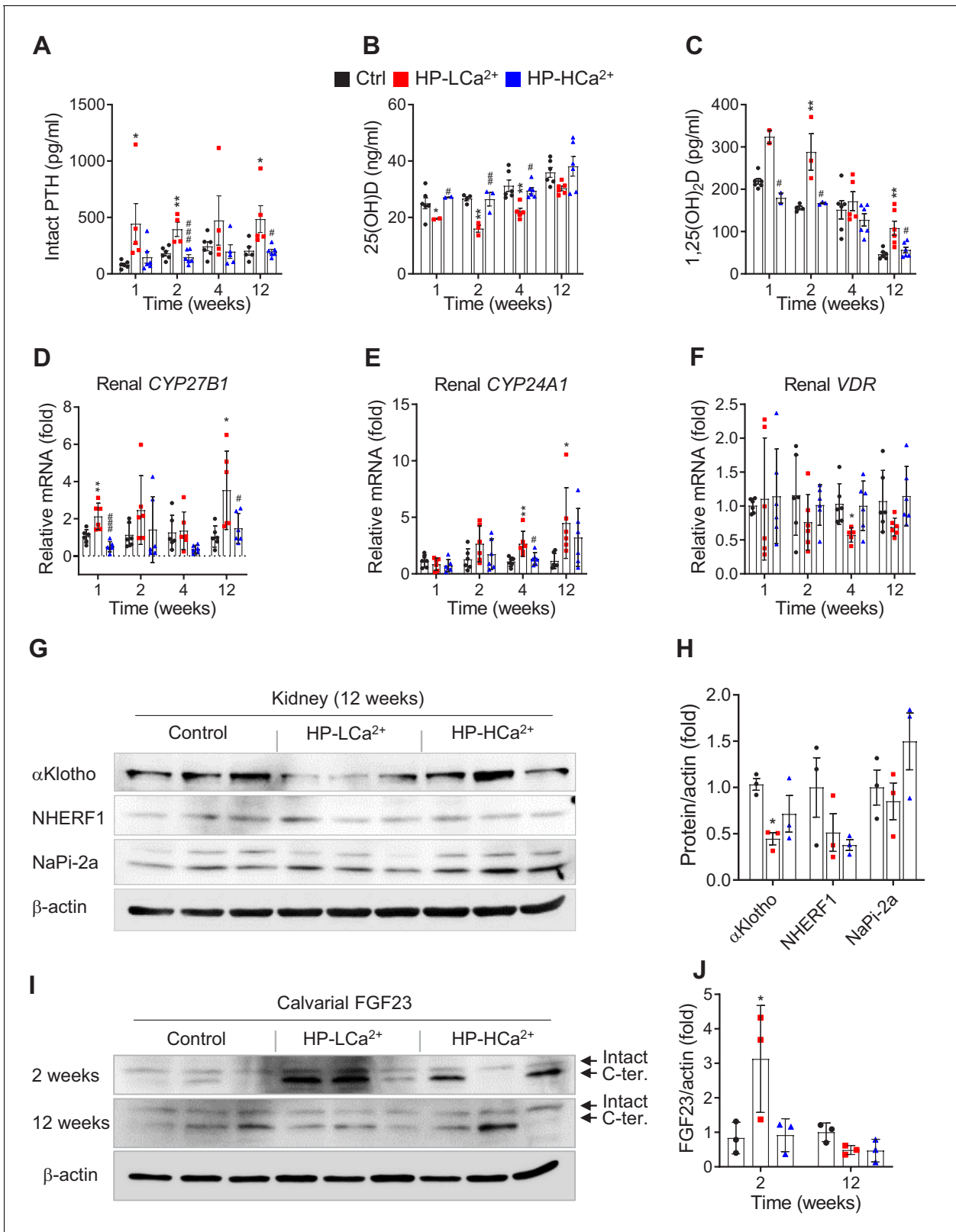


Figure 6. Phytate-mediated Ca²⁺ deficiency promotes vitamin D insufficiency and renal phosphate wasting independent of FGF23 expression. (A–C) Time-course analysis of serum levels of intact PTH (A), 25(OH)D (B), and 1,25(OH)₂D (C) in rats fed control, HP-LCa²⁺, and HP-HCa²⁺ diets. For the early measurement of 25(OH)D (B) and 1,25(OH)₂D, we pooled the sera from 2 to 3 rats. (D–F) Time-course analysis of renal CYP27B1 (D), CYP24A1 (E), and VDR (F) in rats fed control, HP-LCa²⁺, and HP-HCa²⁺ diets. (G) Immunoblot analysis of renal αKlotho, NHERF1, NaPi-2a in rats fed control, HP-LCa²⁺, Figure 6 continued on next page

Figure 6 continued

and HP-HCa²⁺ diets. (H) The levels of renal proteins were quantified using ImageJ software (NIH, Bethesda, MD, USA). (I) Immunoblot analysis of calvarial FGF23 in rats fed control, HP-LCa²⁺, and HP-HCa²⁺ diets. (J) The levels of total calvarial FGF23 were quantified using ImageJ software. All comparisons were conducted using two-way ANOVA with Tukey's post hoc multiple comparison testing or the Kruskal–Wallis test (A–C) for non-parametric statistical analysis of data that did not have a normal distribution. Panels (A–C) failed the normality test, but no outliers were identified. All data are presented as the mean ± SD of each group (n = 4–6 per group). *, p<0.05; **, p<0.01; ***, p<0.001, compared with controls. The online version of this article includes the following figure supplement(s) for figure 6:

Figure supplement 1. High phytate-induced renal phosphate wasting is independent of FGF23.

crystal nephropathy, hypophosphatemia, and bone loss. Our findings support our hypothesis that an HP-LCa²⁺ diet has detrimental metabolic effects on Ca²⁺ and phosphate homeostasis in rats through inhibiting intestinal Ca²⁺ absorption while increasing intestinal phosphate overloading. These events lead to high levels of PTH and low levels of FGF23 and αKlotho. The resulting hypocalcemia and hypophosphatemia caused by the high-phytate/low-Ca²⁺ diet could explain

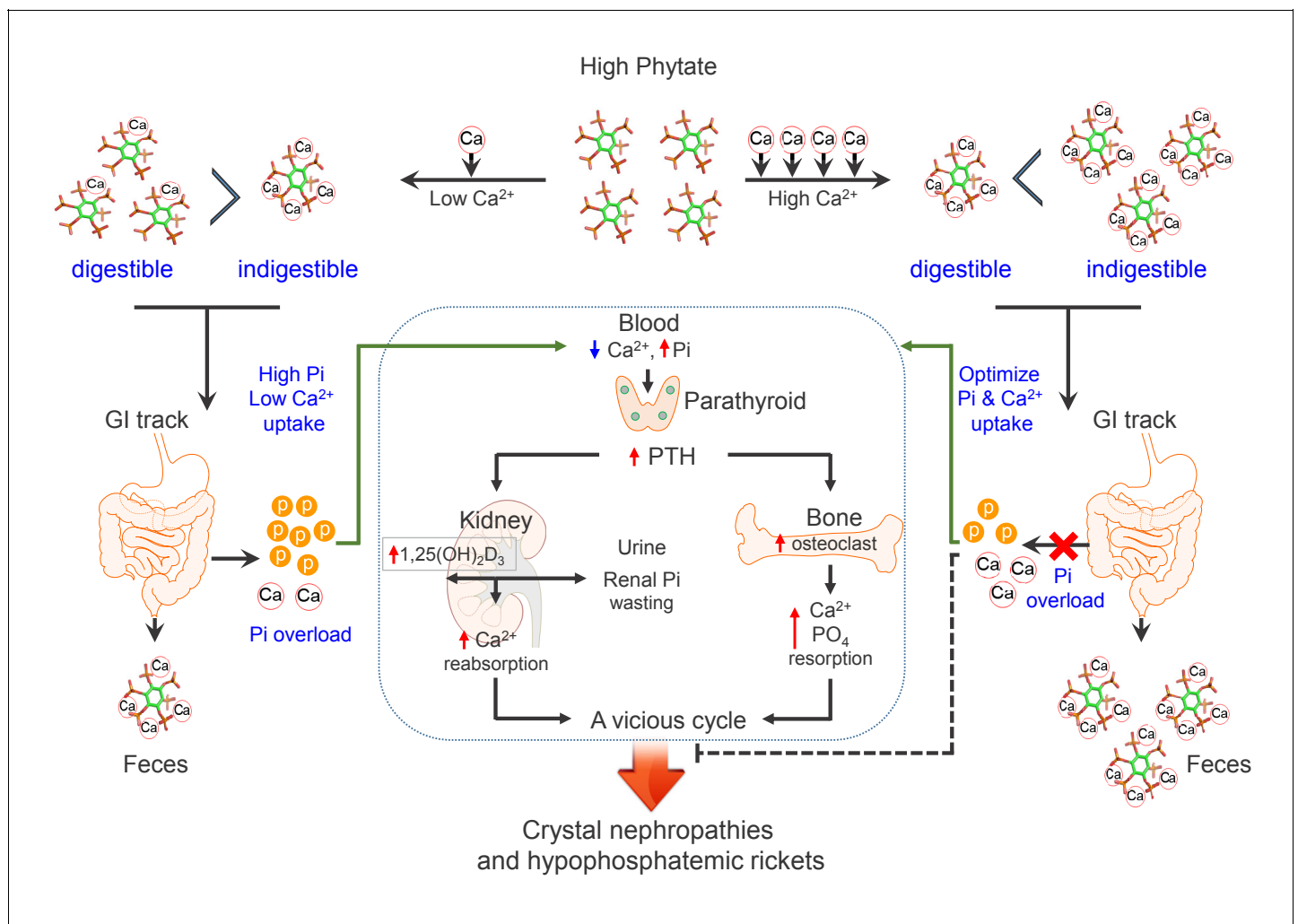


Figure 7. Model for the effects of phytate diets supplemented with low-Ca²⁺ or high-Ca²⁺ on Ca²⁺ and phosphate homeostasis. In the presence of a low-Ca²⁺ diet (Ca²⁺/phytate <5), phytate can adversely affect Ca²⁺ and phosphate homeostasis in normal healthy rats by inhibiting intestinal Ca²⁺ absorption while increasing phosphate overloading through phytate hydrolysis in the intestine. These effects lead to crystal nephropathies, severe renal phosphate wasting, and pathologic bone loss via increased PTH and 1,25(OH)₂D₃. By contrast, in the presence of a high-Ca²⁺ diet, phytate forms multiple Ca²⁺-phytate salts, which makes them indigestible and unabsorbable in vivo, leading to their excretion in the feces as undigested Ca²⁺-phytate salts. This process prevents a vicious cycle of intestinal phosphate overloading and renal phosphate wasting while improving intestinal Ca²⁺ bioavailability, which eventually alleviates the detrimental effects of excess phytate hydrolysis.

the secondary hyperparathyroidism, bone loss and phosphaturia, which in turn causes nephrocalcinosis. By contrast, supplementation with high Ca^{2+} alleviated phytate-mediated pathogenic defects such as biochemical abnormalities, high PTH levels, nephrocalcinosis, renal fibrosis, vitamin D insufficiency, hypophosphatemia, and bone loss. We identified the dietary conditions that influence the bioavailability of phytate when an excess of Ca^{2+} is added to high-phytate diets. Thus, phytate forms insoluble Ca^{2+} -phytate salts in the intestine, where it becomes indigestible and unabsorbable, and ultimately is excreted as undigested Ca^{2+} -phytate salts in the feces. Thus, Ca^{2+} supplementation normalized impaired renal tubular Ca^{2+} and phosphate reabsorption by preventing intestinal phosphate overloading caused by phytate hydrolysis and improving intestinal Ca^{2+} bioavailability (**Figure 7**).

We identified previously unrecognized mechanisms of bioavailability and digestibility of phytate in vivo. Thus, HPIC and ICP-MS analyses of feces revealed that phytate is present in digestible or indigestible forms in vivo depending on the dietary Ca^{2+} content, revealing that phytate is only indigestible and unabsorbable when it forms multiple Ca^{2+} -phytate salts. This finding is consistent with data of our in vitro studies (**Kim et al., 2010**), which show that phytate possesses three or four Ca^{2+} -binding sites at physiological pH and forms insoluble multiple Ca^{2+} -phytate salts. By contrast, when the Ca^{2+} /phytate molar ratio is <5 (HP-LCa²⁺ diet), phytate becomes digestible, which leads to phosphate overloading in the intestine leading to renal phosphate wasting and metabolic bone disease. These results may explain why the adverse effects of high-phytate on nutrients are exacerbated when Ca^{2+} intake or mineral content is low (**Raboy, 2007; Humer et al., 2015**).

Phytases can be classified into two major classes on the basis of their biochemical and structural properties, that is, the histidine acid phytases and the alkaline β -propeller phytases (**Oh et al., 2004; Stentz et al., 2014**). The histidine acid phytase (HAP) superfamily consists of purple acid phosphatase, histidine acid phytase, histidine acid phosphatase, and MINPP1 (**Supplementary file 5**). Our in vivo data suggested that a high-phytate diet can be hydrolyzed and can release excess phosphates into the gut by either mammalian intestinal or microbial MINPP1 when the diet contains a low concentration of Ca^{2+} , although further studies are needed to determine how mammalian MINPP1 is processed and secreted into the digestive tract. The HAPs, predominantly, have positively charged amino acids in their active sites, thereby explaining how the HAPs can bind highly negatively charged phytate at acidic pH but that this is unfavorable for binding to positively charged Ca^{2+} -phytate due to electrostatic repulsion between the Ca^{2+} -phytate and the active sites (**Oh et al., 2004**). This suggests a mechanism to explain why the HAPs can only hydrolyze Ca^{2+} -free phytate but cannot hydrolyze Ca^{2+} -phytate when the diet contains a high concentration of Ca^{2+} , leading to a decrease in the bioaccessibility of Ca^{2+} -phytate and the bioavailability of intestinal phosphates and Ca^{2+} for absorption into the blood, eventually leading to excretion of undigested Ca^{2+} -phytate in the feces. These results explain why high-phytate/high- Ca^{2+} diets prevented the development of crystal nephropathies, renal phosphate wasting, and bone loss in rats. By contrast, β -propeller phytases mainly have negatively charged amino acids in their active sites (**Ha et al., 2000**), which provide a favorable electrostatic environment and strict substrate specificity for the hydrolysis of positively charged Ca^{2+} -phytate but not Ca^{2+} -free phytate, due to electrostatic repulsion between negatively charged phytate and negatively charged amino acids of the active sites (**Supplementary file 5**). Therefore, we propose that humans and other monogastric animals may lack β -propeller phytases that hydrolyze Ca^{2+} -phytate in the gut, as high-phytate/high- Ca^{2+} diets could not be hydrolyzed (indigestible) in the guts of the rats and, eventually, most Ca^{2+} -phytate was excreted in the feces.

Further, the potential toxicity of excess phosphate in the context of mineral bone disorders (MBD) associated with chronic kidney disease (CKD) (**Vervloet et al., 2017; Ketteler et al., 2017**) and Ca^{2+} -phosphate crystals (**Kuro-o, 2013**), together with our present findings, indicate that a HP-LCa²⁺ diet can be particularly harmful to patients suffering from these conditions. Moreover, dietary phosphate overload can cause tubular damage, hypophosphatemia, and Ca^{2+} -phosphate crystals; and phosphate overloading never causes persistent hyperphosphatemia unless renal function is critically impaired (**Haut et al., 1980**). Thus, our study emphasizes that a detailed understanding of the dietary effects and properties of phytate may provide a new opportunity to reduce intestinal phosphate overload and to benefit patients with CKD, mineral bone disease, or crystal nephropathies.

Several lines of evidence support our findings that phytate is digestible in the absence of Ca^{2+} or divalent minerals. First, studies of rats fed ^{14}C -labeled phytate show that approximately 94% of phytate is absorbed when Ca^{2+} intake is low, whereas 54% of phytate is excreted in the feces when Ca^{2+} intake is high (*Nahapetian and Young, 1980*), suggesting that phytate absorption is modulated or inhibited by the Ca^{2+} concentration. Second, another study of rats fed ^3H -inositol phytate shows that 78% of phytate is absorbed and 14% is excreted in the feces. Further, most of the radioactivity represents *myo*-inositol or *myo*-inositol monophosphate in the plasma or urine (*Sakamoto et al., 1993*), suggesting the phytate is digestible *in vivo*. The biased belief that phytate is indigestible led the authors of the above two studies to conclude that intact phytate is absorbed through the upper intestine, hydrolyzed within mucosal cells before entry into the blood, and then released as *myo*-inositol and phosphate into the blood or urine.

Subsequently, investigators who assumed that phytate is absorbed and can be detected in the blood or urine (*Grases et al., 2000*) were unable to detect phytate in serum or urine despite using a highly specific and sensitive mass spectrometry (*Letcher et al., 2008*). These studies support the conclusion that phosphate or *myo*-inositol generated by the hydrolysis of phytate is absorbed rather than phytate, which is unabsorbable. Numerous explanations account for the impermeability of intestinal membranes to phytate (*Reddy and Sathé, 2002*). Phytate possesses six phosphate groups with strong negative charges at physiological pH, which suggests that phytate cannot cross the lipid bilayer of the plasma membrane without a specific receptor (*Ozaki et al., 2000*). In support of this possibility, we found that phytate is only engulfed by hepatic Kupffer cells and tissue macrophages *in vivo* when we intravenously injected iron-containing phytate particles into live mice (*Kim et al., 2017; Lee et al., 2018*), indicating that phytate cannot penetrate membranes of epithelial cells in the intestine. Together, these findings suggest that phytate is not absorbed in the intestine and that only products generated through the hydrolysis of phytate, phosphate, or *myo*-inositol can be absorbed in the intestine of rats fed phytate-containing low- Ca^{2+} diets.

Here, we demonstrate that phytate can act as a dual demon in healthy normal rats by adversely affecting Ca^{2+} and phosphate homeostasis through inhibition of intestinal Ca^{2+} absorption while increasing intestinal phosphate overload, depending on the Ca^{2+} content of diets. This may explain why rats fed the HP-LCa $^{2+}$ diet exhibited high levels of PTH and $1,25(\text{OH})_2\text{D}$, as well as low levels of FGF23 and αKlotho . Moreover, our findings are consistent with data from a large population-based study of subjects with preserved renal function without CKD, which showed that PTH levels increase earlier than FGF23 levels as kidney function decreases and that high FGF23 levels are more closely associated with low levels of $1,25(\text{OH})_2\text{D}$ than with excessive renal phosphate wasting (*Dhayat et al., 2016*). Thus, our results suggest that high levels of $1,25(\text{OH})_2\text{D}$ may suppress the expression of calvarial FGF23 in rats fed the HP-LCa $^{2+}$ diet, in accordance with an earlier study showing that Ca^{2+} deficiency is highly associated with low levels of FGF23 (*Rodriguez-Ortiz et al., 2012*). Moreover, Ca^{2+} deficiency increases the levels of $1,25(\text{OH})_2\text{D}$, which leads to low levels of FGF23 in Ca^{2+} -deficiency states (*Clements et al., 1987*).

However, previous studies that investigated the effects of phytate on kidney stones in rats report conflicting results, which we ascribe to differences in dietary compositions, particularly to the ratio of Ca^{2+} /phytate and analytical laboratory methods (*Grases et al., 2000*). Specifically, the AIN-76A purified rodent diet containing 1% phytate prevents the development of kidney stones compared with the AIN-76A controls (*Grases et al., 2000*). Further, *Grases et al. (2000)* concluded that rats fed the AIN-76A diet developed mineral deposits at the corticomedullary junction from Alizarin Red S staining, whereas *Lien et al. (2001)* did not find an increased incidence or severity of renal tubular mineralization in rats fed the AIN-76A or AIN-93G diet. Consistent with this, we found that rats fed the AIN-93G control diet did not have nephrocalcinosis. Moreover, we found that an AIN-93G-based HP-LCa $^{2+}$ diet induced biochemical and urinary abnormalities associated with kidney disease as well as histopathological defects in the kidney. Phytate in the AIN-96-G diet caused a dramatic time- and concentration-dependent increase in PTH levels, leading to PTH-induced impairment of the renal reabsorption of Ca^{2+} and phosphate, and predisposed rats to the development of hypophosphatemic rickets and nephrocalcinosis.

In conclusion, we demonstrate here that a high-phytate low- Ca^{2+} diet is a risk factor for nephrocalcinosis, renal inflammation, and fibrosis as well as renal phosphate wasting disorders and bone loss in rats. Our studies provide an animal model for studying the pathogenesis of crystal

nephropathies and bone loss associated with renal phosphate wasting, and further suggest that the restriction of phytate intake may reduce the risks of developing crystal nephropathies.

Materials and methods

Key resources table

Reagent type (species) or resource	Designation	Source or reference	Identifiers	Additional information
Genetic reagent (<i>Rattus norvegicus</i>)	Sprague Dawley rat	Orient Bio, Seoul, Korea		Developed by Sprague Dawley, Inc.
Chemical compound, drug	AIN-93G	Dyets Inc.	DYET# 10700	Control diet
Chemical compound, drug	Phytic acid	Sigma-Aldrich	Cat. #: P-8810	Phytate diet
Chemical compound, drug	HNO ₃	Sigma-Aldrich	Cat. #: 438073	Fecal mineral analysis
Chemical compound, drug	HF	Sigma-Aldrich	Cat. #: 695068	Fecal mineral analysis
Chemical compound, drug	HCl	Sigma-Aldrich	Cat. #: H1758	Fecal mineral analysis
Chemical compound, drug	EDTA	Sigma-Aldrich	Cat. #: 93283	Fecal phytate analysis
Chemical compound, drug	NaOH	Sigma-Aldrich	Cat. #: 415413	Fecal phytate analysis
Chemical compound, drug	Calcium	Beckman Coulter	OSR6113	Serum/urine biochemistry
Chemical compound, drug	Phosphate	Beckman Coulter	OSR6122	Serum/urine biochemistry
Chemical compound, drug	BUN (Urea)	Beckman Coulter	OSR6134	Serum/urine biochemistry
Chemical compound, drug	Creatinine	Beckman Coulter	OSR6178	Serum/urine biochemistry
Chemical compound, drug	Magnesium	Beckman Coulter	OSR6189	Serum/urine biochemistry
Chemical compound, drug	Urine protein	Beckman Coulter	OSR6170	Urine biochemistry
Commercial assay or kit	Rat intact PTH	Immutopics	Cat. #: 60–2500	ELISA kit
Commercial assay or kit	Human PTH	Abcam	Cat. #: ab230931	ELISA kit
Commercial assay or kit	Rat soluble RANKL	Immundiagnostik	Cat. #: K1019	ELISA kit
Commercial assay or kit	Rat osteoprotegerin	Alpco Immunoassay	Cat. #: 30–1020	ELISA kit
Commercial assay or kit	Rat intact FGF23	Elabscience	Cat. #: E-EL-R3031	ELISA kit
Commercial assay or kit	Rat C-terminal FGF23	Elabscience	Cat. #: E-EL-RB0377	ELISA kit
Commercial assay or kit	Human FGF23	Elabscience	Cat. #: E-EL-H1116	ELISA kit
Commercial assay or kit	25(OH)-Vitamin D	Abbott/USA	ARCHITECT 25-OH Vitamin D	Chemiluminescence microparticle immunoassay
Commercial assay or kit	1,25-(OH) ₂ vitamin D	DIAsource	1,25(OH) ₂ -VIT, D-RIA-CT/Belgium	Radioimmunoassay

Continued on next page

Continued

Reagent type (species) or resource	Designation	Source or reference	Identifiers	Additional information
Commercial assay or kit	Hematoxylin solution	Thermo scientific	Cat. #: TA-125-MH	H&E staining
Commercial assay or kit	Eosin Y solution	Sigma-Aldrich	Cat. #: 318906	H&E staining
Commercial assay or kit	Alizarin Red S	Sigma-Aldrich	Cat. #:130-22-3	Kidney calcium staining
Commercial assay or kit	Von Kossa stain kit	Abcam	Cat. #:ab150687	Kidney calcium staining
Commercial assay or kit	Trichrome stain kit	Abcam	Cat. #:ab150686	Kidney fibrosis staining
Commercial assay or kit	TRAP kit	Sigma-Aldrich	Cat. #:387A	Bone osteoclast
Commercial assay or kit	Oxalate (oxalic acid) Colorimetric assay kit	BioVision	Cat. #: K663	ELISA kit
Commercial assay or kit	QIAamp Fast DNA Stool Mini Kit	Qiagen	Cat. #:51604	Stool DNA preparation
Commercial assay or kit	THUNDERBIRD SYBR qPCR mix	Toyobo	Cat. #:QPS-101	
Commercial assay or kit	TB Green Premix Ex Taq	TaKaRa	RR420L	
Commercial assay or kit	Antibody diluent with background-reducing components	DaKo	Cat. #:S3022	IHC
Commercial assay or kit	Protein block, serum free	DaKo	Cat. #:X0909	IHC
Commercial assay or kit	Liquid DAB + substrate chromogen system	DaKo	Cat. #:K3468	IHC
Peptide, recombinant protein	Mouse RANKL	R and D Systems	Cat. #:462-TEC-010	In vitro osteoclast
Peptide, recombinant protein	Mouse M-CSF	R and D Systems	Cat. #: 416 ML	In vitro osteoclast
Antibody	Mouse monoclonal β -actin	Santa Cruz	Cat. #: AC-15	WB (1:1000)
Antibody	Rabbit polyclonal FGF23	Bioss	Cat. #: bs-5768R	WB (1:200) IHC (1:100)
Antibody	Rabbit polyclonal α klotho	Novus Biologicals	Cat. #: NBP1-76511	WB (1:500)
Antibody	Rabbit polyclonal SLC34A1/NaPi-2a	Abcam	Cat. #: ab151129	WB (1:500)
Antibody	Rabbit polyclonal SLC34A2/NaPi-2b	LSBio	Cat. #: LS-C782282	IHC (1:100)
Antibody	Rabbit polyclonal α -SMA	Abcam	Cat. #:ab5694	IHC (1:100)
Antibody	Rabbit polyclonal TRPV6	Novus Biologicals	Cat. #: NBP2-32372	IHC (1:100)
Antibody	Rabbit polyclonal MINPP1	LSBio	Cat. #: LS-C368910	IHC (1:100)
Software, algorithm	GraphPad Prism 8.0	GraphPad software		Graph and statistics

Care and feeding of rats

Animal studies were approved by the Center for Animal Care and Use and were performed according to institutional ethics and safety guidelines (LCDI-2008–0019, LCDI-2010–0068, and LCDI-2018–0060). Three-week-old male (60–70 g) and female (50–55 g) Sprague–Dawley rats (Orient Bio, Seoul, Korea) were housed three per cage in a 12:12 hr light-dark cycle with ambient temperature maintained at $22 \pm 2^\circ\text{C}$. The rats were fed AIN-93G (Dyets Inc, Bethlehem, PA, USA) for a 1 week adaptation period and were randomly assigned to control AIN-93G (0% phytate), AIN-93G with 1%, 3%, or 5% sodium phytate (P-8810, Sigma-Aldrich, St. Louis, MO, USA) or AIN-93G with 3% sodium phytate with an additional 0.5% Ca^{2+} ($n = 6\text{--}12$ per group) diet for 12 weeks. All diets had equivalent percentages of carbohydrate, protein, fat, and minerals. Pathogen-free water and food were available ad libitum. Food intake and body weight were recorded weekly.

Biochemical assays

The rats were fasted overnight every 2–3 weeks and anesthetized with isoflurane. Tail vein blood samples were stored at 4°C for 10–20 min and serum was frozen at -80°C . At the end of the experiment, the rats were fasted for 14–16 hr before receiving isoflurane. Abdominal aorta blood was obtained, and urine was collected over 24 hr. The kidneys and femora were dissected and stored at -80°C . Serum biochemical analysis was performed (Model AU-480; Beckman Coulter, Fullerton, CA, USA). Rat intact PTH (Immutopics, San Clemente, CA, USA), human intact PTH (Abcam), soluble RANKL (Imundiagnostik, Bensheim, Germany), osteoprotegerin (Alpco Immunoassay, Salem, NH, USA), rat intact and C-terminal FGF23 (Elabscience, Houston, TX, USA), and human intact FGF23 (Elabscience) were measured using enzyme-linked immunosorbent assay. The serum levels of 25-OH Vitamin D and $1,25(\text{OH})_2$ vitamin D were determined by chemiluminescence microparticle immunoassay (Abbott, Abbott Park, IL) and radioimmunoassay (DIAsource, Louvain-la-Neuve, Belgium), respectively, in the biochemistry laboratory at Green Cross Labcell (Yongin, Korea). According to the manufacturers, the antibodies for 25-OH and $1,25(\text{OH})_2$ vitamin D have cross-reactivity for vitamin D2 and D3 forms of 25-OH and $1,25(\text{OH})_2$ vitamin D, respectively. In our assay, the serum levels of 25-OH vitamin D and $1,25(\text{OH})_2$ vitamin D are the sum of both vitamin D2 and D3 levels. Creatinine clearance (Cl) was calculated as $\text{Cl (ml/min)} = (\text{urine [creatinine]} \times \text{urine vol} \times \text{body wt}) / (\text{serum [creatinine]} \times 24 \times 60)$. The fractional excretion of Ca^{2+} or phosphate was calculated as the $\% \text{FE}_{\text{Ca}}$ or $\text{Pi} = \text{urine [Ca}^{2+} \text{ or phosphate}] \times \text{serum [creatinine]} / (\text{urine [creatinine]} \times \text{serum [Ca}^{2+} \text{ or phosphate]}) \times 100$. TmP/GFR and $\text{TmCa}^{2+}/\text{GFR}$ were calculated in accordance with the Walton and Bijvoet nomogram (Walton and Bijvoet, 1975) using a 24 hr urine sample and a serum sample obtained 16 hr after urine collection and fasting.

Fecal mineral content analysis

Fecal samples were collected from rats after 2 or 4 weeks of either the control or phytate-supplemented diet. Rats were placed in grid cages over clean trays to collect samples. Food was removed from the cages during collection to avoid contamination. All samples were stored at -80°C . Ca^{2+} , magnesium, iron, and phosphate were quantified on an inductively coupled plasma optical emission spectrometer (Optima 5300 DV; PerkinElmer, Waltham, MA, USA). Fecal samples were dried at 60°C for 48 hr, and 1.0 g was heated at 560°C for 4 hr. After cooling to room temperature, 1 mL of 35.5% HNO_3 was added and samples were heated at 560°C for an additional 2 hr. Samples were then exposed to 4 mL 17.5% HCl at room temperature for 2 hr before dilution in ultra-pure water. Fecal phytate was sequentially extracted with a HCl-HF acid solution, followed by an alkaline extraction (NaOH and EDTA), as previously described (Ray et al., 2012). The phytate content of fecal extracts was quantified by high-performance ion chromatography (ICS-3000; Dionex).

Kidney histopathology

Hematoxylin and eosin (HE)-stained kidney sections ($n = 64$) from eight male and eight female rats were blindly examined by one author (CJB). Ca^{2+} was stained with Alizarin Red S and von Kossa. Sections obtained from females were stained with Periodic acid–Schiff. Parameters were scored semiquantitatively on the basis of previous work (Laloti et al., 2006). The measured parameters included the presence and severity of mineralization, inflammation, tubular casts, tubular ectasia, interstitial fibrosis, tubular degeneration/regeneration, and glomerular hypertrophy (0 = negative or

within normal limits, 1 = minimal, 2 = mild, 3 = moderate, 4 = marked, and 5 = severe). Individual scores were added together for each kidney, with a maximum score of 40.

In vivo magnetic resonance imaging (MRI)

We used a 9.4 T animal MRI scanner (Biospec 94/20 USR; Bruker Biospin, Ettlingen, Germany) with a transmit-only volume coil for excitation and phased-array four-channel surface coil for signal reception (Bruker Biospin). Animals were anesthetized using isoflurane. MRI scans were performed using the following respiratory-gated, fat-suppressed gradient echo sequence: TR/TE, 5000/28.5 ms; FA, 180°; FOV, 70 × 60 mm²; matrix size, 384 × 384; TH, 1.0 mm; 27 slices (no gap); and NEX, 4. Axial images were acquired for anatomic reproducibility and histopathological correlation.

Bone mineral density (BMD)

The right femora samples were harvested from eight mice per group after 12 weeks on either control or phytate-supplemented diet. Ex vivo BMD, bone mineral content, and femoral lengths were measured by peripheral dual-energy X-ray absorptiometry (pDEXA) (Sabre; Norland Medical Systems Corp., Fort Atkinson, WI, USA) with pDEXA Sabre software (version 3.9.4; Norland). Scans of femora (4 × 4 cm²) were performed at 3 mm/s and resolution of 0.2 × 0.2 mm. BMD was computed using dual X-ray beam attenuation (28 and 48 KeV), and BMD histogram averaging widths were 0.02 g/cm². In vitro precision, expressed as the coefficient of variation (CV = 100 × standard deviation/mean), was calculated by the BMD of a phantom with a nominal density of 0.929 g/cm².

μ-computed tomography (μ-CT) analysis

The femora were isolated from soft tissue, fixed overnight in 10% formalin, and analyzed by high-resolution μ-CT (SkyScan1172 in vivo CT; Bruker). Imaging (NRecon ver. 1.6; Bruker), data analysis (CTAn ver. 1.11; Bruker), and three-dimensional visualization (μ-CTVol ver. 2.2) were performed on 500 slices per scan at 70 kVp, 141 μA, and 11.55 μm pixel⁻¹. Cross-sectional images were obtained for three-dimensional histomorphometry. A 1.2 mm sample of metaphyseal secondary spongiosa was imaged. Cross-sectional images (500 images per specimen) of distal femora were used for two-dimensional and three-dimensional morphometry.

Bone histomorphometry

The right femora were fixed in 10% formalin for 48 hr, decalcified with 8% hydrochloric acid/formic acid for 2 weeks, and embedded in paraffin. Longitudinally oriented 2.5 μm thick bone sections (including metaphyses and diaphyses) were processed for HE and Masson's trichrome stains. The left femora were fixed in formalin for 48 hr, decalcified in 10% EDTA (pH 7.0) for 4–5 weeks at 4°C, and embedded in paraffin for tartrate-resistant acid phosphatase staining. Sections were viewed using a Zeiss Axio Imager Z1 microscope (Carl Zeiss, Oberkochen, Germany). Histomorphometric measurements were made at the center of the metaphyses. Images were captured with 3DHISTECH (Budapest, Hungary). Bone sections (2.5 μm thick) were stained with Masson's trichrome for osteoids.

Rat bone marrow osteoclasts

Bone marrow cells were isolated using a modified method (Kobayashi et al., 2000). Tibiae and femora were isolated from rats after 12 weeks on either control or phytate-supplemented diet. Bone ends were removed and the marrow was flushed by slowly injecting serum-free alpha minimal essential medium (αMEM; Invitrogen, Carlsbad, CA, USA) through a sterile 25-gauge needle into one end of the bone. Marrow cells were collected into tubes, washed twice with αMEM, and cultured in αMEM with 10% heat-inactivated fetal bovine serum (Invitrogen). Cells were cultured in 24-well plates (1 × 10⁵/well) with 30 ng/mL of macrophage colony-stimulating factor (M-CSF) for 72 hr. Differentiation of M-CSF-dependent bone marrow osteoclast precursors was induced with 30 ng/mL receptor activator of nuclear factor kappa-B ligand (RANKL) (R and D Systems, Minneapolis, MN, USA) and 30 ng/mL M-CSF for 4 days. Differentiated osteoclasts with more than three nuclei were identified as tartrate-resistant acid phosphatase-positive (Leukocyte Acid Phosphatase Assay, Sigma).

Western blotting and immunohistochemistry (IHC)

The primary antibodies used for Western blotting or immunohistochemistry were monoclonal β -actin (AC-15, 1:1000; Santa Cruz), FGF23 (bs-5768R, 1:200; Bioss), α Klotho (NBP1-76511, 1:500; Novus Biologicals), NHERF1 (A-7, 1:200; Santa Cruz), NaPi-2a (ab182099, 1:500; Abcam), and NaPi-2a (ab151129, 1:500; Abcam), as described previously (*Kang et al., 2017*). Antigen retrieval for IHC was performed in Tris/EDTA (pH 9.0) for 2–3 min. IHC was performed with the following antibodies at 25°C for 2 hr: α -SMA (ab5694, 1:100; Abcam), NaPi-2b (S ab182099, 1:100; Abcam), TMPV6 (NBP2-32372, 1:100; Novus Biologicals), MINPP1 (LS-C368910, 1: 100; LSBio), or FGF23 (bs-5768R, 1:200; Bioss). Horseradish peroxidase-conjugated secondary antibodies were detected with 3,3'-diamino-benzidine tetrahydrochloride substrate (Dako, Glostrup, Denmark). All sections were counterstained with hematoxylin (Thermo Scientific).

qRT-PCR analyses

Total RNA was extracted from whole kidney lysates with Trizol (Invitrogen). cDNA synthesis and real-time RT-PCR were performed using TB Green Premix Ex Taq cDNA Synthesis kit (TaKaRa Bio, Tokyo, Japan) with 1 μ g total RNA plus random hexamers in BioRad CFX384. All expression values were normalized to the *cyclophilin A* mRNA level. Primer sequences are listed in *Supplementary file 6*.

Phytate pilot study in humans

A noncomparative pilot study was approved by the Institutional Review Board of Dongguk University Ilsan Hospital (IRB No. 2014–117). All procedures were performed in accordance with the Declaration of Helsinki. The study was registered with Clinical Research Information Service (registration number KCT0003144) in accordance with the WHO International Clinical Trials Registry Platform. This study aimed to evaluate the effects of phytate intake on mineral metabolism in humans between January and February 2015. All participants provided written informed consent. In total, six premenopausal women aged between 23 and 34 years with a body mass index between 17.7 and 25.8 kg/m² were recruited. The exclusion criteria were as follows: bone and mineral metabolism disorders (e.g., hyperparathyroidism, hypoparathyroidism, osteomalacia); previous surgical history which could affect bone and mineral metabolism (e.g., parathyroidectomy, thyroidectomy, and gastrectomy); use of any medication that could affect bone and mineral metabolism (e.g., estrogen, bisphosphonates, selective estrogen receptor modulators, and calcitonin); use of Ca²⁺ and vitamin D supplementation within the past 3 months; use of corticosteroids within the past 1 month; acute or chronic renal failure; exhibited abnormal liver function; or people who were pregnant or lactating. All participants completed a 12-day trial consisting of three successive diet cycles containing: (1) polished rice (low phytate content, 0.35%); (2) brown rice (medium phytate content, 1.07%); and (3) brown rice mixed with rice bran (high phytate content, 2.17%). Each diet cycle lasted for 4 days. During each day of the study, all participants were provided with breakfast, lunch, dinner, and a snack. Every meal was packed in a lunch box and delivered each day, and participants were not allowed to consume any other food during the trial except for the food provided by study investigators. All meals were identical across the three diet cycles except for the phytate content. Water consumption was allowed ad libitum. No medications or supplements that affected mineral metabolism were allowed during the course of the study. A blood sample was collected from each participant at the beginning of the trial and at the end of each diet cycle. Urine samples of 24 hr were collected before the trial and during the fourth day of each diet cycle.

Microbiota analysis

Genomic DNA was isolated from frozen stool samples using the QIAamp fast DNA stool kit (Qiagen, Valencia, CA) according to the manufacturer's instructions. Levels of 16S rRNA gene expression of each bacterial phylum were quantified using THUNDERBIRD SYBR qPCR mix (Toyobo, Osaka, Japan) on a CFX Connect real-time PCR detection system (Bio-Rad, Hercules, CA).

Statistical analysis

Sample sizes for all experiments were based on preliminary results and previous experience of conducting related experiments. Power calculations were not used to determine sample sizes. Animals for each group of experiments were randomly assigned. No animals were excluded from statistical

analysis, and investigators were blinded to the study condition when scoring histopathological samples. Unless noted otherwise, all data are presented as the mean \pm standard deviation (SD). Statistical comparisons of groups were performed by either unpaired Student's *t* test or one-way ANOVA with Tukey's post hoc multiple comparison test. All data were subjected to D'Agostino and Pearson ($n > 8$) or Shapiro–Wilk ($n < 8$) normality test before analysis. Those groups that failed the normality test ($p < 0.05$) were subjected to an outlier test (ROUT; $Q = 1\%$), as recommended to determine whether the outlier was responsible for the failure of the normality test. If the exclusion of outliers led to passing the normality test and altered the statistical results, the exclusion was made; if it did not alter the statistical outcome, no data were excluded from that group. The Kruskal–Wallis test was used for non-parametric statistical analysis of data that did not have a normal distribution. We performed data analysis and prepared graphs using GraphPad Prism 8.0 (GraphPad Software Inc, San Diego, CA).

Acknowledgements

The authors thank Dr S Dhe-Paganon and S Shoelson at Harvard Medical School for their valuable suggestions regarding the manuscript.

Additional information

Funding

Funder	Grant reference number	Author
National Research Foundation of Korea	2017R1D1A1B03031094	Ok-Hee Kim
National Research Foundation of Korea	2019R1A2C2008130	Byung-Chul Oh
Ministry of Food and Drug Safety	14182MFDS460	Byung-Chul Oh
Korea Health Industry Development Institute	HI14C1135	Byung-Chul Oh
Ministry of Food and Drug Safety	16181MFDS381	Byung-Chul Oh

The funders had no role in study design, data collection and interpretation, or the decision to submit the work for publication.

Author contributions

Ok-Hee Kim, Conceptualization, Data curation, Funding acquisition, Writing - original draft, Writing - review and editing; Carmen J Booth, Young Jae Lee, Cheol Soon Lee, Cheolsoo Choi, Yun Jae Jung, Sun Wook Cho, Data curation, Formal analysis; Han Seok Choi, Data curation, Formal analysis, Investigation; Jinwook Lee, Investigation; Jinku Kang, June Hur, Formal analysis, Investigation; Woo Jin Jung, Yun-Shin Jung, Hyung Jin Choi, Hyeonjin Kim, Joong-Hyuck Auh, Data curation; Jung-Wan Kim, Ji-Young Cha, Seung-Soon Im, Formal analysis; Jun-Young Yang, Resources, Formal analysis; Dae Ho Lee, Conceptualization, Formal analysis, Writing - review and editing; Young-Bum Kim, Kyong Soo Park, Conceptualization, Formal analysis; Young Joo Park, Conceptualization, Formal analysis, Writing - original draft, Writing - review and editing; Byung-Chul Oh, Conceptualization, Formal analysis, Funding acquisition, Writing - original draft, Project administration, Writing - review and editing

Author ORCIDs

Byung-Chul Oh  <https://orcid.org/0000-0002-4277-7083>

Ethics

Clinical trial registration A noncomparative pilot study was approved by the Institutional Review Board of Dongguk University Ilsan Hospital (IRB No. 2014-117). All procedures were performed in

accordance with the Declaration of Helsinki. The study was registered with Clinical Research Information Service (registration number KCT0003705; https://cris.nih.go.kr/cris/en/search/search_result_st01.jsp?seq=13397) in accordance with the WHO International Clinical Trials Registry Platform. This study aimed to evaluate the effects of phytate intake on mineral metabolism in humans between January and February 2015.

Human subjects: A noncomparative pilot study was approved by the Institutional Review Board of Dongguk University Ilsan Hospital (IRB No. 2014-117). All procedures were performed in accordance with the Declaration of Helsinki. The study was registered with Clinical Research Information Service (registration number KCT0003705; https://cris.nih.go.kr/cris/en/search/search_result_st01.jsp?seq=13397) in accordance with the WHO International Clinical Trials Registry Platform. This study aimed to evaluate the effects of phytate intake on mineral metabolism in humans between January and February 2015. All participants provided written informed consent. In total, six premenopausal women aged between 23 and 34 years with a body mass index between 17.7 and 25.8 kg/m² were recruited. The exclusion criteria were as follows: bone and mineral metabolism disorders (e.g., hyperparathyroidism, hypoparathyroidism, osteomalacia), previous surgical history which could affect bone and mineral metabolism (e.g., parathyroidectomy, thyroidectomy, gastrectomy), use of any medication that could affect bone and mineral metabolism (e.g., estrogen, bisphosphonates, selective estrogen receptor modulators, calcitonin), use of Ca²⁺ and vitamin D supplementation within the past 3 months, use of corticosteroids within the past 1 month, or acute or chronic renal failure; exhibited abnormal liver function; or were pregnant or lactating.

Animal experimentation: Animal studies were approved by the Center for Animal Care and Use and were performed according to institutional ethics and safety guidelines (LCDI-2008-0019, LCDI-2010-0068, and LCDI-2018-0060).

Decision letter and Author response

Decision letter <https://doi.org/10.7554/eLife.52709.sa1>

Author response <https://doi.org/10.7554/eLife.52709.sa2>

Additional files

Supplementary files

- Supplementary file 1. Composition of the AIN-93G rodent diets for experimental studies with rats.
- Supplementary file 2. The nutrient compositions for three different diets.
- Supplementary file 3. Biochemical properties during three consecutive diets.
- Supplementary file 4. Phylum- and class-specific primers for real-time PCR.
- Supplementary file 5. Biochemical and structural properties of mammalin, gut microbial, and bacterial phytases.
- Supplementary file 6. The qRT-PCR primer lists.
- Transparent reporting form

Data availability

Our primer lists are provided in Supplementary files 4 and 6, and the summary of in a dietary study of humans is provided as Supplementary file 2.

References

- Aggarwal V**, Seth A, Aneja S, Sharma B, Sonkar P, Singh S, Marwaha RK. 2012. Role of calcium deficiency in development of nutritional rickets in Indian children: a case control study. *The Journal of Clinical Endocrinology & Metabolism* **97**:3461–3466. DOI: <https://doi.org/10.1210/jc.2011-3120>, PMID: 22893720
- Al Hasan SM**, Hassan M, Saha S, Islam M, Billah M, Islam S. 2016. Dietary phytate intake inhibits the bioavailability of iron and calcium in the diets of pregnant women in rural Bangladesh: a cross-sectional study. *BMC Nutrition* **2**:24. DOI: <https://doi.org/10.1186/s40795-016-0064-8>

- Calvo MS**, Kumar R, Heath H. 1988. Elevated secretion and action of serum parathyroid hormone in young adults consuming high phosphorus, low calcium diets assembled from common foods. *The Journal of Clinical Endocrinology & Metabolism* **66**:823–829. DOI: <https://doi.org/10.1210/jcem-66-4-823>, PMID: 2831248
- Chan SSL**, Ferguson EL, Bailey K, Fahmida U, Harper TB, Gibson RS. 2007. The concentrations of iron, calcium, zinc and phytate in cereals and legumes habitually consumed by infants living in east Lombok, Indonesia. *Journal of Food Composition and Analysis* **20**:609–617. DOI: <https://doi.org/10.1016/j.jfca.2007.03.003>
- Cho J**, Choi K, Darden T, Reynolds PR, Pettitte JN, Shears SB. 2006. Avian multiple inositol polyphosphate phosphatase is an active phytase that can be engineered to help ameliorate the planet's "phosphate crisis". *Journal of Biotechnology* **126**:248–259. DOI: <https://doi.org/10.1016/j.jbiotec.2006.04.028>, PMID: 16759730
- Clements MR**, Johnson L, Fraser DR. 1987. A new mechanism for induced vitamin D deficiency in calcium deprivation. *Nature* **325**:62–65. DOI: <https://doi.org/10.1038/325062a0>
- Dhayat NA**, Ackermann D, Pruijm M, Ponte B, Ehret G, Guessous I, Leichtle AB, Paccaud F, Mohaupt M, Fiedler GM, Devuyst O, Pechère-Bertschi A, Burnier M, Martin PY, Bochud M, Vogt B, Fuster DG. 2016. Fibroblast growth factor 23 and markers of mineral metabolism in individuals with preserved renal function. *Kidney International* **90**:648–657. DOI: <https://doi.org/10.1016/j.kint.2016.04.024>, PMID: 27370409
- Ellis R**, Kelsay JL, Reynolds RD, Morris ER, Moser PB, Frazier CW. 1987. Phytate:zinc and phytate X calcium:zinc millimolar ratios in self-selected diets of americans, asian indians, and nepalese. *Journal of the American Dietetic Association* **87**:1043–1047. PMID: 3611550
- Ford JA**, Colhoun EM, McIntosh WB, Dunnigan MG. 1972. Biochemical response of late rickets and osteomalacia to a chupatty-free diet. *BMJ* **3**:446–447. DOI: <https://doi.org/10.1136/bmj.3.5824.446>, PMID: 5069221
- Golovan SP**, Hayes MA, Phillips JP, Forsberg CW. 2001. Transgenic mice expressing bacterial phytase as a model for phosphorus pollution control. *Nature Biotechnology* **19**:429–433. DOI: <https://doi.org/10.1038/88091>, PMID: 11329011
- Goswami R**, Gupta N, Goswami D, Marwaha RK, Tandon N, Kochupillai N. 2000. Prevalence and significance of low 25-hydroxyvitamin D concentrations in healthy subjects in delhi. *The American Journal of Clinical Nutrition* **72**:472–475. DOI: <https://doi.org/10.1093/ajcn/72.2.472>, PMID: 10919943
- Grases F**, Prieto RM, Simonet BM, March JG. 2000. Phytate prevents tissue calcifications in female rats. *BioFactors* **11**:171–177. DOI: <https://doi.org/10.1002/biof.5520110303>, PMID: 10875304
- Ha NC**, Oh BC, Shin S, Kim HJ, Oh TK, Kim YO, Choi KY, Oh BH. 2000. Crystal structures of a novel, thermostable phytase in partially and fully calcium-loaded states. *Nature Structural Biology* **7**:147–153. DOI: <https://doi.org/10.1038/72421>, PMID: 10655618
- Haines RW**, Zolfaghari P, Wan Y, Pearse RM, Puthuchery Z, Prowle JR. 2019. Elevated urea-to-creatinine ratio provides a biochemical signature of muscle catabolism and persistent critical illness after major trauma. *Intensive Care Medicine* **45**:1718–1731. DOI: <https://doi.org/10.1007/s00134-019-05760-5>, PMID: 31531715
- Harrison DC**, Mellanby E. 1939. Phytic acid and the rickets-producing action of cereals. *Biochemical Journal* **33**:1660–1680. DOI: <https://doi.org/10.1042/bj0331660>
- Haut LL**, Alfrey AC, Guggenheim S, Buddington B, Schrier N. 1980. Renal toxicity of phosphate in rats. *Kidney International* **17**:722–731. DOI: <https://doi.org/10.1038/ki.1980.85>, PMID: 7412107
- Huang X**, Jiang Y, Xia W. 2013. FGF23 and phosphate wasting disorders. *Bone Research* **1**:120–132. DOI: <https://doi.org/10.4248/BR201302002>, PMID: 26273497
- Humer E**, Schwarz C, Schedle K. 2015. Phytate in pig and poultry nutrition. *Journal of Animal Physiology and Animal Nutrition* **99**:605–625. DOI: <https://doi.org/10.1111/jpn.12258>, PMID: 25405653
- Iqbal TH**, Lewis KO, Cooper BT. 1994. Phytase activity in the human and rat small intestine. *Gut* **35**:1233–1236. DOI: <https://doi.org/10.1136/gut.35.9.1233>, PMID: 7959229
- Jariwalla RJ**, Sabin R, Lawson S, zS H. 1990. Lowering of serum cholesterol and triglycerides and modulation of divalent cations by dietary phytate. *Journal of Applied Nutrition* **42**:18–28.
- Kang JK**, Kim OH, Hur J, Yu SH, Lamichhane S, Lee JW, Ojha U, Hong JH, Lee CS, Cha JY, Lee YJ, Im SS, Park YJ, Choi CS, Lee DH, Lee IK, Oh BC. 2017. Increased intracellular Ca²⁺ concentrations prevent membrane localization of PH domains through the formation of Ca²⁺-phosphoinositides. *PNAS* **114**:11926–11931. DOI: <https://doi.org/10.1073/pnas.1706489114>, PMID: 29078297
- Karim Z**, Gérard B, Bakouh N, Alili R, Leroy C, Beck L, Silve C, Planelles G, Urena-Torres P, Grandchamp B, Friedlander G, Prié D. 2008. *NHERF1* mutations and responsiveness of renal parathyroid hormone. *New England Journal of Medicine* **359**:1128–1135. DOI: <https://doi.org/10.1056/NEJMoa0802836>, PMID: 18784102
- Ketteler M**, Block GA, Evenepoel P, Fukagawa M, Herzog CA, McCann L, Moe SM, Shroff R, Tonelli MA, Toussaint ND, Vervloet MG, Leonard MB. 2017. Executive summary of the 2017 KDIGO chronic kidney Disease-Mineral and Bone Disorder (CKD-MBD) Guideline Update: what's changed and why it matters. *Kidney International* **92**:26–36. DOI: <https://doi.org/10.1016/j.kint.2017.04.006>, PMID: 28646995
- Kim OH**, Kim YO, Shim JH, Jung YS, Jung WJ, Choi WC, Lee H, Lee SJ, Kim KK, Auh JH, Kim H, Kim JW, Oh TK, Oh BC. 2010. β -propeller phytase hydrolyzes insoluble Ca²⁺-phytate salts and completely abrogates the ability of phytate to chelate metal ions. *Biochemistry* **49**:10216–10227. DOI: <https://doi.org/10.1021/bi1010249>, PMID: 20964370
- Kim OH**, Kim H, Kang J, Yang D, Kang YH, Lee DH, Cheon GJ, Park SC, Oh BC. 2017. Impaired phagocytosis of apoptotic cells causes accumulation of bone marrow-derived macrophages in aged mice. *BMB Reports* **50**:43–48. DOI: <https://doi.org/10.5483/BMBRep.2017.50.1.167>, PMID: 27866511
- Kobayashi K**, Takahashi N, Jimi E, Udagawa N, Takami M, Kotake S, Nakagawa N, Kinoshita M, Yamaguchi K, Shima N, Yasuda H, Morinaga T, Higashio K, Martin TJ, Suda T. 2000. Tumor necrosis factor alpha stimulates

- osteoclast differentiation by a mechanism independent of the ODF/RANKL-RANK interaction. *Journal of Experimental Medicine* **191**:275–286. DOI: <https://doi.org/10.1084/jem.191.2.275>, PMID: 10637272
- Kong Y-Y**, Yoshida H, Sarosi I, Tan H-L, Timms E, Capparelli C, Morony S, Oliveira-dos-Santos AJ, Van G, Itie A, Khoo W, Wakeham A, Dunstan CR, Lacey DL, Mak TW, Boyle WJ, Penninger JM. 1999. OPG is a key regulator of osteoclastogenesis, lymphocyte development and lymph-node organogenesis. *Nature* **397**:315–323. DOI: <https://doi.org/10.1038/16852>
- Kronenberg F**. 2009. Emerging risk factors and markers of chronic kidney disease progression. *Nature Reviews Nephrology* **5**:677–689. DOI: <https://doi.org/10.1038/nrneph.2009.173>, PMID: 19935815
- Kumar V**, Sinha AK, Makkar HPS, Becker K. 2010. Dietary roles of phytate and phytase in human nutrition: A review. *Food Chemistry* **120**:945–959. DOI: <https://doi.org/10.1016/j.foodchem.2009.11.052>
- Kuro-o M**. 2013. Klotho, phosphate and FGF-23 in ageing and disturbed mineral metabolism. *Nature Reviews Nephrology* **9**:650–660. DOI: <https://doi.org/10.1038/nrneph.2013.111>, PMID: 23774819
- Lacey DL**, Timms E, Tan HL, Kelley MJ, Dunstan CR, Burgess T, Elliott R, Colombero A, Elliott G, Scully S, Hsu H, Sullivan J, Hawkins N, Davy E, Capparelli C, Eli A, Qian YX, Kaufman S, Sarosi I, Shalhoub V, et al. 1998. Osteoprotegerin ligand is a cytokine that regulates osteoclast differentiation and activation. *Cell* **93**:165–176. DOI: [https://doi.org/10.1016/S0092-8674\(00\)81569-X](https://doi.org/10.1016/S0092-8674(00)81569-X), PMID: 9568710
- Lalioti MD**, Zhang J, Volkman HM, Kahle KT, Hoffmann KE, Toka HR, Nelson-Williams C, Ellison DH, Flavell R, Booth CJ, Lu Y, Geller DS, Lifton RP. 2006. Wnk4 controls blood pressure and potassium homeostasis via regulation of mass and activity of the distal convoluted tubule. *Nature Genetics* **38**:1124–1132. DOI: <https://doi.org/10.1038/ng1877>, PMID: 16964266
- Lee JH**, Phelan P, Shin M, Oh BC, Han X, Im SS, Osborne TF. 2018. SREBP-1a-stimulated lipid synthesis is required for macrophage phagocytosis downstream of TLR4-directed mTORC1. *PNAS* **115**:E12228–E12234. DOI: <https://doi.org/10.1073/pnas.1813458115>, PMID: 30530672
- Letcher AJ**, Schell MJ, Irvine RF. 2008. Do mammals make all their own inositol hexakisphosphate? *Biochemical Journal* **416**:263–270. DOI: <https://doi.org/10.1042/BJ20081417>, PMID: 18684107
- Lien EL**, Boyle FG, Wrenn JM, Perry RW, Thompson CA, Borzelleca JF. 2001. Comparison of AIN-76A and AIN-93G diets: a 13-week study in rats. *Food and Chemical Toxicology* **39**:385–392. DOI: [https://doi.org/10.1016/S0278-6915\(00\)00142-3](https://doi.org/10.1016/S0278-6915(00)00142-3), PMID: 11295485
- Mellanby E**. 1949. The rickets-producing and anti-calcifying action of phytate. *The Journal of Physiology* **109**:488–533. DOI: <https://doi.org/10.1113/jphysiol.1949.sp004411>, PMID: 15395027
- Moe SM**, Zidehsarai MP, Chambers MA, Jackman LA, Radcliffe JS, Trevino LL, Donahue SE, Asplin JR. 2011. Vegetarian compared with meat dietary protein source and phosphorus homeostasis in chronic kidney disease. *Clinical Journal of the American Society of Nephrology* **6**:257–264. DOI: <https://doi.org/10.2215/CJN.05040610>, PMID: 21183586
- Monico CG**, Milliner DS. 2012. Genetic determinants of urolithiasis. *Nature Reviews Nephrology* **8**:151–162. DOI: <https://doi.org/10.1038/nrneph.2011.211>
- Mulay SR**, Anders HJ. 2017. Crystal nephropathies: mechanisms of crystal-induced kidney injury. *Nature Reviews Nephrology* **13**:226–240. DOI: <https://doi.org/10.1038/nrneph.2017.10>, PMID: 28218266
- Nahapetian A**, Young VR. 1980. Metabolism of ¹⁴C-Phytate in Rats: Effect of Low and High Dietary Calcium Intakes. *The Journal of Nutrition* **110**:1458–1472. DOI: <https://doi.org/10.1093/jn/110.7.1458>
- Nair AB**, Jacob S. 2016. A simple practice guide for dose conversion between animals and human. *Journal of Basic and Clinical Pharmacy* **7**:27–31. DOI: <https://doi.org/10.4103/0976-0105.177703>, PMID: 27057123
- Oh BC**, Choi WC, Park S, Kim YO, Oh TK. 2004. Biochemical properties and substrate specificities of alkaline and histidine acid phytases. *Applied Microbiology and Biotechnology* **63**:362–372. DOI: <https://doi.org/10.1007/s00253-003-1345-0>, PMID: 14586576
- Oh BC**, Kim MH, Yun BS, Choi WC, Park SC, Bae SC, Oh TK. 2006. Ca(2+)-inositol phosphate chelation mediates the substrate specificity of beta-propeller phytase. *Biochemistry* **45**:9531–9539. DOI: <https://doi.org/10.1021/bi0603118>, PMID: 16878987
- Onomi S**, Okazaki Y, Katayama T. 2004. Effect of dietary level of phytic acid on hepatic and serum lipid status in rats fed a high-sucrose diet. *Bioscience, Biotechnology, and Biochemistry* **68**:1379–1381. DOI: <https://doi.org/10.1271/bbb.68.1379>, PMID: 15215609
- Ozaki S**, DeWald DB, Shope JC, Chen J, Prestwich GD. 2000. Intracellular delivery of phosphoinositides and inositol phosphates using polyamine carriers. *PNAS* **97**:11286–11291. DOI: <https://doi.org/10.1073/pnas.210197897>, PMID: 11005844
- Pettifor JM**. 1994. Privational rickets: a modern perspective. *Journal of the Royal Society of Medicine* **87**:723–725. PMID: 7853292
- Raboy V**. 2000. Low-phytic-acid grains. *Food and Nutrition Bulletin* **21**:423–427. DOI: <https://doi.org/10.1177/156482650002100416>
- Raboy V**. 2007. The ABCs of low-phytate crops. *Nature Biotechnology* **25**:874–875. DOI: <https://doi.org/10.1038/nbt0807-874>, PMID: 17687363
- Ray PP**, Shang C, Maguire RO, Knowlton KF. 2012. Quantifying phytate in dairy digesta and feces: alkaline extraction and high-performance ion chromatography. *Journal of Dairy Science* **95**:3248–3258. DOI: <https://doi.org/10.3168/jds.2011-4984>, PMID: 22612959
- Razzaque MS**. 2009. The FGF23-Klotho Axis: endocrine regulation of phosphate homeostasis. *Nature Reviews Endocrinology* **5**:611–619. DOI: <https://doi.org/10.1038/nrendo.2009.196>, PMID: 19844248
- Reddy NR**, Sathe SK, Salunkhe DK. 1982. Phytates in legumes and cereals. *Advances in Food Research* **28**:1–92. DOI: [https://doi.org/10.1016/s0065-2628\(08\)60110-x](https://doi.org/10.1016/s0065-2628(08)60110-x), PMID: 6299067

- Reddy NR**, Sathe SH. 2002. *Food Phytates*. CRC Press.
- Rodriguez-Ortiz ME**, Lopez I, Muñoz-Castañeda JR, Martínez-Moreno JM, Ramírez AP, Pineda C, Canalejo A, Jaeger P, Aguilera-Tejero E, Rodriguez M, Felsenfeld A, Almaden Y. 2012. Calcium deficiency reduces circulating levels of FGF23. *Journal of the American Society of Nephrology* **23**:1190–1197. DOI: <https://doi.org/10.1681/ASN.2011101006>, PMID: 22581996
- Sakamoto K**, Vucenik I, Shamsuddin AM. 1993. [³H]phytic acid (inositol hexaphosphate) is absorbed and distributed to various tissues in rats. *The Journal of Nutrition* **123**:713–720. DOI: <https://doi.org/10.1093/jn/123.4.713>, PMID: 8463873
- Shavit L**, Jaeger P, Unwin RJ. 2015. What is nephrocalcinosis? *Kidney International* **88**:35–43. DOI: <https://doi.org/10.1038/ki.2015.76>, PMID: 25807034
- Stentz R**, Osborne S, Horn N, Li AW, Hautefort I, Bongaerts R, Rouyer M, Bailey P, Shears SB, Hemmings AM, Brearley CA, Carding SR. 2014. A bacterial homolog of a eukaryotic inositol phosphate signaling enzyme mediates cross-kingdom dialog in the mammalian gut. *Cell Reports* **6**:646–656. DOI: <https://doi.org/10.1016/j.celrep.2014.01.021>, PMID: 24529702
- Thompson LU**, Button CL, Jenkins DJ. 1987. Phytic acid and calcium affect the in vitro rate of navy bean starch digestion and blood glucose response in humans. *The American Journal of Clinical Nutrition* **46**:467–473. DOI: <https://doi.org/10.1093/ajcn/46.3.467>, PMID: 3630965
- Uchino S**, Bellomo R, Goldsmith D. 2012. The meaning of the blood urea nitrogen/creatinine ratio in acute kidney injury. *Clinical Kidney Journal* **5**:187–191. DOI: <https://doi.org/10.1093/ckj/sfs013>, PMID: 29497527
- Vervloet MG**, Sezer S, Massy ZA, Johansson L, Cozzolino M, Fouque D, ERA–EDTA Working Group on Chronic Kidney Disease–Mineral and Bone Disorders and the European Renal Nutrition Working Group. 2017. The role of phosphate in kidney disease. *Nature Reviews Nephrology* **13**:27–38. DOI: <https://doi.org/10.1038/nrneph.2016.164>, PMID: 27867189
- Walton RJ**, Bijvoet OLM. 1975. Nomogram for derivation of renal threshold phosphate concentration. *The Lancet* **306**:309–310. DOI: [https://doi.org/10.1016/S0140-6736\(75\)92736-1](https://doi.org/10.1016/S0140-6736(75)92736-1)
- Wesseling-Perry K**, Pereira RC, Tseng CH, Elashoff R, Zaritsky JJ, Yadin O, Sahney S, Gales B, Jüppner H, Salusky IB. 2012. Early skeletal and biochemical alterations in pediatric chronic kidney disease. *Clinical Journal of the American Society of Nephrology* **7**:146–152. DOI: <https://doi.org/10.2215/CJN.05940611>, PMID: 22052943